

The Pennsylvania State University
The Graduate School
Department of Material Science and Engineering

**INFLUENCE OF CARBON SPACERS AND ALKYL PENDANT CHAINS ON THE
STABILITY OF QUATERNARY AMMONIUM CATIONS FOR ANION EXCHANGE
MEMBRANES**

A Thesis in
Material Science and Engineering

by
Clara Capparelli

© 2015 Clara Capparelli

Submitted in Partial Fulfillment
of the Requirements
for the Degree of

Master of Science

August 2015

The thesis of Clara Capparelli was reviewed and approved* by the following:

Michael A. Hickner
Associate Professor of Materials Science and Engineering
Thesis Advisor

James Runt
Professor of Polymer Science

T.C. Mike Chung
Professor of Material Science and Engineering

Suzanne Mohny
Professor of Material Science and Engineering and Electrical Engineering
Chair, Intercollege Graduate Degree Program in Material Science and
Engineering

*Signatures are on file in the Graduate School

ABSTRACT

Proton and anion exchange membranes are of great importance in the function of fuel cells, one of the most promising technologies for renewable energy conversion. Proton exchange membrane fuel cells (PEMFC) have been studied extensively in the past couple of decades, and there have been tremendous advances in the development of these systems, especially in industries such as automotive and portable power. Anion exchange membranes (AEM) have caught the attention of scientists because they would allow for the development of fuel cells without costly precious metal catalysts, among other advantages. Efforts are being made in developing long-lived and high performance AEMs for fuel cell applications.

Primarily, the focus in AEM research has been membrane stability. It has been observed that AEMs are not as stable as the state-of-the-art NAFION[®] PEM and demonstrations of cell performance beyond 1000 hours is rare. For this reason, scientists are in the search for more stable AEMs. The first step to developing more stable membranes is to understand the mechanisms by which these membranes degrade – both in ex-situ and in-situ stability assessments. It is the focus of this thesis to provide insight in the degradation mechanisms of AEMs under highly basic conditions.

The topic of this thesis is the use of alkyl spacers between the polymeric backbone and cationic group, and alkyl pendant chains replacing one of the methyl groups in the quaternary ammonium moiety, to provide steric hindrance around the cation and lower the degradation rate of the nitrogen-centered cation. Samples were developed with systematically differing architectures, for example, different lengths of alkyl spacers. The samples were then degraded under highly basic conditions at high temperatures. The strategy chosen to detect degradation was the analysis of the degradation by-products of the degraded small molecules, by two different

characterization techniques: ^1H NMR and LC-MS. ^1H NMR was chosen to provide quantitative information of the degradation rates of various analogue small molecules with distinct chemistries; LC-MS was chosen to identify the degradation by-products and thus, determine the degradation mechanisms. These results on small molecules can be extended to membranes as described in some preliminary membrane experiments and in future work.

It is the aim of this work to deeply probe the steric hindrance strategy to stable ammonium cations as well as provide a clear methodology for determining the degradation rates and mechanisms of analogue small molecules for AEMs.

TABLE OF CONTENTS

List of Figures	v
List of Tables	vi
Acknowledgements.....	vii
Chapter 1 Introduction	1
Chapter 2 Literature Review	7
Introduction.....	7
Fuel cells	7
Anion Exchange Membranes	10
Introduction	10
Polymer backbone	10
Cationic groups	11
Stability of Anion Exchange Membranes	14
Degradation mechanisms	14
Alkyl spacers for enhanced stability	18
Pendant chains.....	22
Nuclear Magnetic Resonance (NMR).....	23
Theory of Nuclear Magnetic Resonance	23
¹ H NMR and stability of AEMs	25
Liquid Chromatography Mass Spectrometry	27
Liquid Chromatography	27
Mass Spectrometry	28
LC-MS in polymer degradation	29
Summary	32
Chapter 3 Experimental procedures for sample preparation and characterization.....	35
Introduction.....	35
Synthesis of Small Molecule Cations as Analogues for AEM Degradation	35
Degradation experiments	39
Liquid Chromatography Mass Spectrometry Analysis	41
¹ H Nuclear Magnetic Resonance Spectroscopy	43
Summary	43
Chapter 4 The influence of alkyl spacers and pendant chains on the stability of small molecules analogues for Anion Exchange Membranes by ¹ H NMR	45
Introduction.....	45
Stability	46
Conclusions.....	52

Chapter 5 Identification of degradation mechanisms by LC-MS	54
Introduction.....	54
Identification of degradation by-products and mechanisms	54
Summary	67
Chapter 6 Analysis of degradation by-products of a PPO-based AEM.....	68
Chapter 7 Conclusions and future work.....	73
Conclusions	73
Future work.....	74
Appendix A ¹ H NMR spectrums and degradation mechanisms for each sample	76

LIST OF FIGURES

Figure 1-1. Comparison between PEMFC (left) and AEMFC (right).	2
Figure 1-2. An example of a typical AEM, PPO-BTMA. A $-\text{CH}_3$ in the PPO has been replaced with a benzyl trimethyl quaternary ammonium group.....	3
Figure 1-3. Two different degradation pathways for BTMA. (a) Hydroxide attack in the benzyl carbon forms a benzyl alcohol and trimethylamine as by-products. (b) Hydroxide attack in the methyl carbon forms benzyldimethylamine and methanol as by-products.....	4
Figure 1-4. Hofmann elimination mechanism occurs in the presence of β -Hydrogens.	5
Figure 2-1. PEMFC schematic (left) and AEMFC schematic (right).	9
Figure 2-2. Poly(sulfone) (left), poly(styrene) (center) and poly(phenylene oxide) (right) as materials for AEM backbones.	11
Figure 2-3. Ammonium (left), phosphonium (center) and sulfonium (right) groups as cationic groups for AEM.....	11
Figure 2-4. Alkaline stability of different cations functionalized to PSF at 1 M KOH, 60°C	12
Figure 2-5. Study on relative stability of benzyltrimethylammonium chloride (left) and 1-benzyl-3-methylimidazolium (right) performed by Varcoe et al.	13
Figure 2-6. FT-Raman spectra of 1-benzyl-3-methylimidazolium chloride (bottom) and benzyltrimethylammonium chloride (top) after 14 days in heat treatment reveals decrease intensity in the imidazolium-related bands.....	13
Figure 2-7. Nucleophilic substitution mechanism.	15
Figure 2-8. Elimination mechanism.....	15
Figure 2-9. Dealkylation mechanism.	16
Figure 2-10. Substitution mechanism.	16
Figure 2-11. Hofmann elimination mechanism.	17
Figure 2-12. Anion exchange resins. R' indicates spacer chains.	19
Figure 2-13. Thermal stability of alkyleneoxymethylene spacer-modified anion exchangers.....	20

Figure 2-14. Poly(phenylene)s with benzylic cations studied by Hibbs.....	21
Figure 2-15. Poly(phenylene)s with sidechain tethered cations studied by Hibbs.....	21
Figure 2-16. Changes in chloride ion conductivity during test in 4 M KOH at 90°C.....	22
Figure 2-17. Hydroxide conductivity at 20°C as a function of ion exchange capacity (left) and changing trend in IEC values after immersion in 1 M NaOH at 80°C.....	23
Figure 2-18. ¹ H NMR spectrum of ethyl acetate, intensity versus chemical shift.	25
Figure 2-19. Comparison of ¹ H NMR spectrums of an imidazolium-based membrane before and after stability test.	26
Figure 2-20. Degradation profile from 1H NMR spectra for small molecule imidazolium salts in 1 M NaOH in 4:1 D2O:CD3OD at 60°C for 48 hours.....	26
Figure 2-21. General scheme of a mass spectrometer.....	29
Figure 2-22. Degradation pathways of the small molecule imidazolium salt.	30
Figure 2-23. MS of the model compound after the alkaline stability test.....	30
Figure 2-24. LC chromatographic trace of degraded model compound.	31
Figure 2-25. MS spectra of LC trace of degraded model compound product mixture at different elution times.	32
Figure 3-1. Small Molecule Cations synthesized for degradation experiment, from left to right, BTMA, 3QA1, 4QA1, 6QA1 and 3QA6 in their salt form.	36
Figure 3-2. Synthetic route used for samples BTMA, 3QA1, 4QA1 and 6QA1, with <i>n</i> being 1, 3, 4 and 6 respectively.....	37
Figure 3-3. Synthetic route used for sample 3QA6.	38
Figure 3-4. Fluoride test performed on the PTFE vials. Color scale shows test discs from 0 to 100 mg/L of F ⁻ . Comparison of discs used to analyze solution after degradation treatment reveals 0 mg/L of F ⁻	40
Figure 3-5. Gradient profile used in the LC-MS acquisition program.....	42
Figure 4-1. Small molecules with various lengths of alkyl spacers and pendant chains used for this work.....	46
Figure 4-2. Comparison of spectrums from time 0 to time 48 hours on BTMA sample.	47
Figure 4-3. TMA degradation profile in BTMA sample.	48
Figure 4-4. TMA degradation profile in 6QA1 sample.	49

Figure 4-5. Degradation profile of BTMA, 3QA1, 4QA1, 6QA1 and 3QA6 in the presence of NaOH (20 equivalents) at 120°C over 48 hours.	49
Figure 4-6. Plot of the rate of degradation of samples BTMA (◆), 3QA1 (■), 4QA1 (▲), 6QA1 (+) and 3QA6 (●).	51
Figure 5-1. TIC of sample 4QA1 at time 0 (top) and time 24 h (bottom).	56
Figure 5-2. Spectrum of sample 4QA1 at time 0, at retention time 10.10 minutes.	57
Figure 5-3. TIC (top), EICs for the non-degraded compound and the two degradation by-products and spectrum at retention time 3.14 minutes (bottom) for sample BTMA.	58
Figure 5-4. TIC (top), EICs for the non-degraded compound and the two degradation by-products and spectrum at retention time 10.27 minutes (bottom) for sample 3QA1.	60
Figure 5-5. TIC and EICs for sample 4QA1 at time point 24 hours.	62
Figure 5-6. TIC and EICs for sample 6QA1 at time point 24 hours.	64
Figure 5-7. TIC and EICs for sample 3QA6 at time point 24 hours.	66
Figure 6-1. PPO-1QA6.	68
Figure 6-2. ¹ H NMR spectrum at time zero (blue) and 72 hours (red).	69
Figure 6-3. ¹ H NMR spectrum at 120 hours.	70
Figure 6-4. COSY NMR spectrum at 120 hours.	70
Figure 6-5. COSY NMR spectrum, closer look at region 0.4 – 1.5 ppm.	71
Figure 6-6. Substitution mechanism in PPO-1QA6.	72
Figure A-1. NMR spectrum for sample BTMA. The peak at 3.17 ppm is suspected to be an impurity.	76
Figure A-2. NMR spectrum for sample 3QA1.	76
Figure A-3. NMR spectrum for sample 4QA1.	77
Figure A-4. NMR for sample 6QA1.	77
Figure A-5. NMR for 3QA6.	78
Figure A-6. Degradation mechanisms for sample BTMA.	79
Figure A-7. Degradation mechanisms for sample 3QA1.	80
Figure A-8. Degradation mechanisms for sample 4QA1.	81

Figure A-9. Degradation mechanisms for sample 6QA1.....	82
Figure A-10. Degradation mechanisms for sample 3QA6.....	83
Figure A-11. Degradation profile of the TMA moiety for sample 3QA1.....	84
Figure A-12. Degradation profile of the TMA moiety for sample 4QA1.....	85
Figure A-13. Degradation profile of the TMA moiety for sample 3QA6.....	86

LIST OF TABLES

Table 2-1. Spacer chains utilized for the anion exchange resins.	19
Table 3-1. Exact amounts of starting materials for samples BTMA, 3QA1, 4QA1 and 6QA1.....	37
Table 3-2. Starting materials for sample 3QA6.	38
Table 3-3. Experimental setup for each of the samples.	39
Table 3-4. Exact masses of the degradation by-products of the samples.....	42
Table 4-1. Degradation constants and half-lives of samples BTMA, 3QA1, 4QA1, 6QA1 and 3QA6.	51
Table 5-1. Degradation by-products of samples by LCMS.	67

ACKNOWLEDGEMENTS

I am very thankful for the help and support that I received during this past two years; I couldn't have completed my degree without it.

First of all, I want to thank the Argentinian Presidency and the Fulbright Commission for giving me the amazing opportunity of expanding my knowledge in such an important university as Penn State. I will keep this last two years in my heart forever. I want to thank Prof. Hickner for the opportunity of joining his group, for being a source of inspiration, for giving me freedom in my research as well as giving me guidance when I needed it.

Second, I want to thank Sean Nunez, Brandon Calitree and Caroline Christensen for helping me in my first year in the Hickner Group. I want to thank them for helping me with my research, for showing me how to use equipment, for helping me understand how everything worked in this university. A special thanks to Carlos Pacheco, for helping me with my NMR measurements, always with a smile, and for showing interest in my work.

I want to thank the friends I made in the group, Doug, T.J., Sarah and Harrison, for making it all more fun, for making me laugh, for making the office a nice place where to be, for showing interest in my culture, for being good friends to have a beer with and also, to discuss research with. I want to thank the rest of the Hickner group for making such a nice group of people, for being smart and hardworking, but always having a smile and being respectful to each other.

Third, I want to thank the friends I made in State College: my Chilean friends Felipe, Natalie, Josefina and Ignacio, my Uruguayan friend Lucilla, my fellow countryman Bernardo, my Ecuadorian friends Miguel and Steffanie, my Mexican friends Ilse, Miguel, baby Antonella, Iker, Isa, Sandra and Wil, for being such good friends, for helping us when we first got here, for showing me their culture and understanding mine, for the parties, the holidays, the dinners, the

trips and all the fun activities we had together. I love knowing that I leave State College with more friends that I came with. I am thankful for coming to a place with such diversity!

I am also thankful for my family in Argentina, my mom Fernanda, my dad Lolo, my grandmother Lili and my grandfather Miguel, and all the rest of my family, for giving me their support to come here, for missing me a lot, but being happy for my personal and professional growth. Thanks to all my family for believing in me and being proud of me.

And last but not least, I want to thank my husband Junior, for being such an inspirational person. Thanks for travelling 10,000 miles for me and with me, thanks for being fearless and courageous, and coming to a country where you didn't know the language, for being so positive and overcome any obstacles you found, for finding your own path here and for being so unique. Thank you for making me a better person every day. I love you with all my heart and I am beyond happy of spending the rest of my life with you.

Thanks to everyone who helped me succeed in my studies, I couldn't have done it without you.

Chapter 1

Introduction

The search for clean energy sources and energy conversion technology has become one of the most important topics among the scientific community for the benefit of our society. With an increasing population worldwide, the global energy consumption is projected to increase 56% from 2010 to 2040, according to the International Energy Outlook 2013¹. Additionally, according to the United States Environmental Protection Agency (EPA), electricity production was responsible in 2013 for 31% of the greenhouse gas emissions², which create significant and harmful impacts on the environment and our health. In contrast, most renewable energy source generate little to no global warming emissions. The need for cleaner, renewable energy sources has become undeniable and fuel cells are one of the promising components of clean energy systems. The U.S. Office of Energy Efficiency & Renewable Energy considers that fuel cells can address critical challenges in all energy sectors, including commercial, industrial and transportation, while offering a broad range of benefits for the environment and the nation's energy security, not only by reducing the greenhouse gas emissions as mentioned before, but also by reducing oil consumption, air pollution and expanding the use of renewable power³.

In fuel cells, electrical energy is generated by an electrochemical reaction between hydrogen and oxygen, with heat and water as the only by-products. Among the various types of fuel cells, proton exchange membrane fuel cells (PEMFC) and anion exchange membrane fuel cells (AEMFC) are two of the most important technologies in low-temperature, mobile systems. In PEMFCs, hydrogen is oxidized to form two protons (H^+) and two electrons (e^-). The electrons generate the current in an external circuit and the protons are transported through a proton

exchange membrane (PEM) from the anode to the cathode. At the cathode, protons and electrons reduce oxygen from air and form water. In AEMFCs, hydroxide ions (OH^-) are transported through an anion exchange membrane (AEM) from cathode to anode, opposite to PEMFC, where they recombine with protons to generate water (see Figure 1-1).

PEMFCs require the use of expensive Pt-based catalysts for the reactions to occur, while the higher pH in AEMFCs makes costly precious metals catalysts unnecessary. There is less corrosion at higher pH and the non-precious metal catalysts can be inexpensive. However, AEM show less stability than that achieved for PEMs currently.

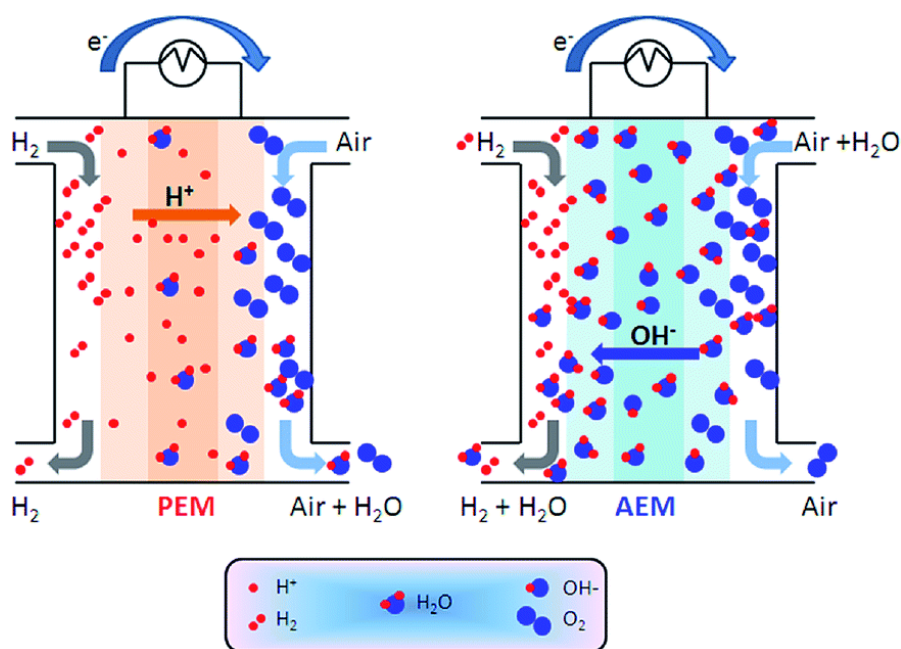


Figure 1-1. Comparison between PEMFC (left) and AEMFC (right)⁴.

An AEM consists of a polymeric backbone with pendant cation groups. Several membrane chemistries have been studied, and typical polymer backbones include poly(styrene) (PS), poly(sulfones) (PES) and poly(phenylene oxide) (PPO). Among the cationic groups tethered

to the backbones, the most widely used are benzyl trimethyl quaternary ammonium (BTMA) groups (QA) (see Figure 1-2 for BTMA QA-PPO).

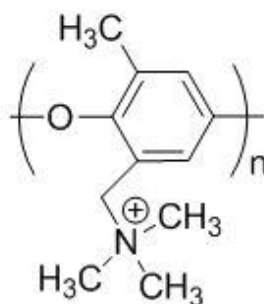


Figure 1-2. An example of a typical AEM, PPO-BTMA. A -CH_3 in the PPO has been replaced with a benzyl trimethyl quaternary ammonium group.

The stability of the AEM depends of both the polymer backbone and the tethered cationic group. It is hypothesized that degradation occurs via OH^- attack, but other reactive oxygen species in an electrochemical environment cannot be ruled out during device operation. Polymer backbones chemistries, like PES, PS and PPO, were studied and PPO showed comparable stabilities to PS and much better stability than PES⁵. As for the cationic head-group, different architectures are still under consideration for an optimized AEM. As mentioned before, BTMA shows promising AEM capabilities because of its alkaline stability, low cost and ease of synthesis. However, BTMA as presented in Figure 1-2 undergoes degradation under accelerated conditions of high base concentration and high temperature. The positive charge of the nitrogen attracts the electrons further apart from the alpha carbons, creating partial positive charges over these carbons, making them prone to hydroxide attack. Two different degradation pathways are shown in Figure 1-3 for the quaternary ammonium analogue *benzyltrimethylammonium* (BTMA). If the hydroxide attacks the benzyl carbon, then the QA group is displaced and a benzyl alcohol is

formed (a). If the hydroxide attacks the methyl carbon, *benzyltrimethylammonium* and *methanol* are formed as by-products (b).

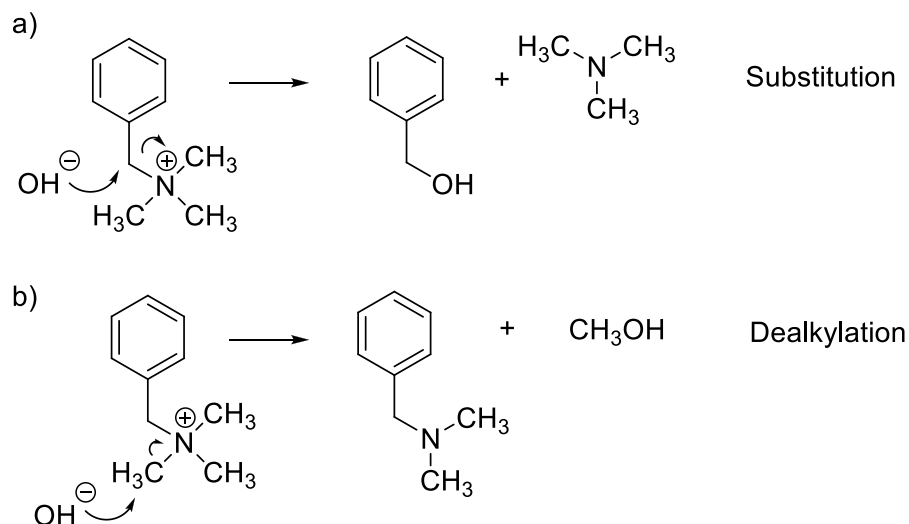


Figure 1-3. Two different degradation pathways for BTMA. (a) Hydroxide attack in the benzyl carbon forms a benzyl alcohol and trimethylamine as by-products. (b) Hydroxide attack in the methyl carbon forms benzyltrimethylamine and methanol as by-products.

Both these reactions are substitution type reactions (S_N2) and in the presence of a β -hydrogen, the cationic group can undergo an elimination type reaction (E_1) also known as Hofmann elimination. The OH^- attacks the β -hydrogen to the nitrogen leaving to form a molecule of water. The electrons then form a double bond between the α and β carbon forming an alkene. The remaining pair of electrons at the α -carbon create a stable *benzylamine*, as seen in Figure 1-4.

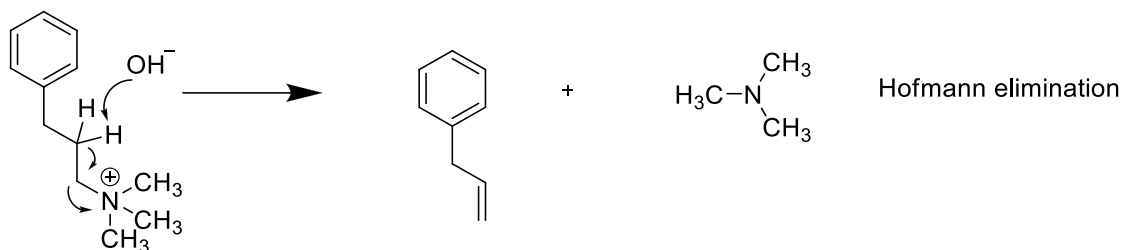


Figure 1-4. Hofmann elimination mechanism occurs in the presence of β -Hydrogens.

Other degradation mechanisms can also take place, depending on the structure of the ammonium group, such as Stevens rearrangement, Sommetlet-Hausser rearrangement and 1,4-elimination⁶. Degradation is thought to occur because of the electrophilic character of the QA, enhanced by the presence of the adjacent electron-withdrawing benzyl group⁷. Several strategies have been developed to decrease the pressure on the adjacent carbons by either charge delocalization or steric hindrance⁸. Charge delocalization strategies include the use of imidazolium or guanidinium as the cationic groups, but they have shown rapid degradation in alkaline media. For this reason, Kreuer concluded that steric hindrance to lower the reactivity of the QA is one of the most promising strategies to achieve high stabilities in AEM. One means of acquiring steric hindrance is by the addition of an alkyl spacer between the QA and the polymer backbone. Another approach is by addition of a terminal alkyl chain pendant to the QA. It is logical to expect that a cation with both architectures shows exceptional stability.

The aim of this work is to understand the extent of the influence of alkyl spacers and pendant chains on stability for AEM applications. This work examines different cationic architectures in order to identify the best strategies for increased stability. Moreover, it is the intention of this work to characterize the different degradation pathways by identifying the degradation products in the presence of base. The analysis is simplified by investigating analogue small molecules under mimic fuel cell conditions – high temperature and presence of strong base – to identify possible new chemistries for AEM.

-
1. Energy Information Administration, World Energy Outlook 2013, page 1.
[http://www.eia.gov/forecasts/ieo/pdf/0484\(2013\).pdf](http://www.eia.gov/forecasts/ieo/pdf/0484(2013).pdf)
 2. Environmental Protection Agency, 2012. <http://www.epa.gov/climatechange/ghgemissions/sources.html>
 3. Office of Energy Efficiency & Renewable Energy, Fuel Cells. <http://energy.gov/eere/fuelcells/about-fuel-cell-technologies-office>
 4. Varcoe, J. R., Atanassov, P., Dekel, D. R., Herring, A. M., Hickner, M. A., Kohl, P. A., ... & Zhuang, L. Anion-exchange membranes in electrochemical energy systems. *Energy & Environmental Science* **2014**, 7(10), 3135-3191.
 5. Li, N., Leng, Y., Hickner, M. A., & Wang, C. Y. (2013). Highly stable, anion conductive, comb-shaped copolymers for alkaline fuel cells. *Journal of the American Chemical Society*, 135(27), 10124-10133.
 6. Ye, Yuesheng, and Yossef A. Elabd. "Relative chemical stability of imidazolium-based alkaline anion exchange polymerized ionic liquids." *Macromolecules* **2011**, 44.21, 8494-8503.
 7. Marino, M. G., & Kreuer, K. D. Alkaline Stability of Quaternary Ammonium Cations for Alkaline Fuel Cell Membranes and Ionic Liquids. *ChemSusChem* **2014**.
 8. Kreuer, K. D. Ion conducting membranes for fuel cells and other electrochemical devices. *Chemistry of Materials* **2013**, 26(1), 361-380.

Chapter 2

Literature Review

Introduction

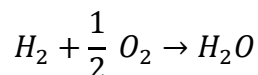
This chapter will provide a review and analysis of the literature consulted for this work. It will begin with a description of fuel cells and their main features. Different types of fuel cells will be described and Anion Exchange Membrane Fuel Cells (AEMFC) will be explained in more detail. The advantages of AEMFC over other types of fuel cells will be explained, altogether with the challenges that need to be addressed to utilize them as everyday technology. Membrane stability and degradation mechanisms will be described, as well as strategies for achieving enhanced stability. Since Liquid Chromatography Mass Spectrometry (LC-MS) and Nuclear Magnetic Resonance (NMR) were used to study degradation rates and mechanisms, a review of these characterization techniques is included, as well as previous studies that use LC-MS and NMR to characterize degradation.

Fuel cells

Fuel cells are one of the most promising technologies in the search for new, clean energy conversion devices. A fuel cell is a device that converts the chemical energy of a fuel into electricity by an electrochemical reaction. There are different designs of fuel cells, but they all consist of three main components: two electrodes, the anode and the cathode, which are separated by the electrolyte. At the anode, the direct oxidation of hydrogen or the oxidation of methanol occurs. At the cathode, the oxygen is reduced, in most cases from air. The net reaction is the

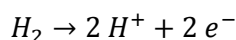
formation of a molecule of water with the generation of heat and electrons, which in a closed external circuit generate the current (Equation 1).

Equation 1

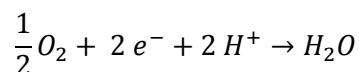


Some fuel cells are divided according to the type of electrode and which species it transports. Fuel cells with a proton conducting electrolyte are known as Proton Exchange Membrane Fuel Cells (PEMFC, Figure 2-1, left). In this type of devices, hydrogen is oxidized at the anode into protons and electrons (Equation 2)¹. The electrons flow in the external circuit and the protons are transported through the membrane and to the cathode. At the cathode, oxygen from air is recombined with the protons and electrons to generate water (Equation 3).

Equation 2

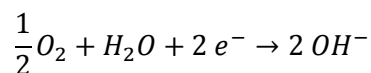


Equation 3

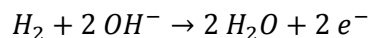


In an AEMFC, Figure 2-1 right, hydroxide ions (OH^-) instead of protons are generated in the cathode (Equation 4) and transported to the anode where they recombine with hydrogen to generate water (Equation 5).

Equation 4



Equation 5



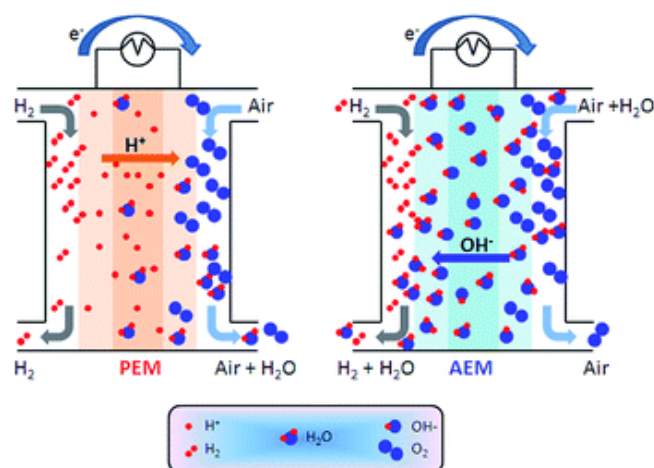


Figure 2-1. PEMFC schematic (left) and AEMFC schematic (right)⁴.

In both types of fuel cells, the electrolyte is a solid membrane that is responsible for transporting the ions from one electrode to the other, depending on the type of device, as described before. In an AEMFC, the electrolyte consists of a membrane (Anion Exchange Membrane, AEM) that selectively allows the passage of hydroxide ions from the cathode and transports it to the anode. AEMs will be described in more depth in the next section.

In PEMFCs, the oxidation reaction of hydrogen occurs very fast on Pt-based catalysts, while the high pH of AEMFC allows for the use of a low level of Pt catalyst or a cheaper non-precious metal one². Also, AEMFCs allow for an extended range of materials and a wider choice of fuels in addition to H₂. However, the disadvantages related with AEM include low OH⁻ conductivities³ and low stability in the highly alkaline environment created by the presence of OH⁻ groups⁴. Research on AEM has focused on these two critical aspects for achieving great device performances.

Anion Exchange Membranes

Introduction

An AEM consists of a polymer backbone with tethered cationic groups. The AEM functions as the electrolyte in an AEMFC and it allows the transport of hydroxide ions from the cathode to the anode, as shown in Figure 2-1. For this reason, it is essential for the membrane to have high ionic conductivity; however, conductivities for AEMs reported early in the literature show significantly lower conductivity than that of protons for PEMFC. It has become evident that the low hydroxide conductivity in AEMFC is caused in part by CO₂ contamination, which causes the conversion of hydroxide ions into carbonates (CO₃²⁻) and bicarbonates (HCO₃⁻)⁵. Other important requirements for fuel cell application are good mechanical properties, high stability in the alkaline media, provide effective anode/cathode separation, carrier for hydroxyl transport and low cost. This work will focus on different strategies to achieve high stability. In order to achieve high overall stability in the AEM, stability of the backbone and cationic group are both required⁶, while maintaining the functionality of the cationic groups.

Polymer backbone

Typical polymer backbone architectures include poly(styrene) (PS), poly(phenylene oxide) (PPO), and poly(arylene ether sulfone) (PSF)⁷, Figure 2-2.

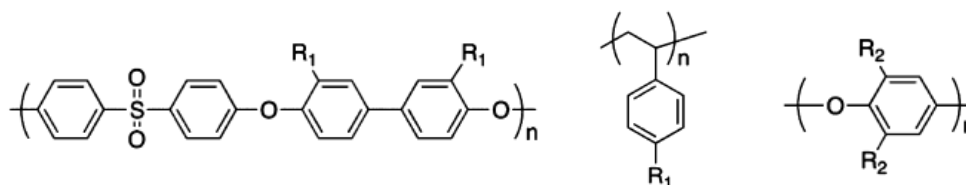


Figure 2-2. Poly(sulfone) (left), poly(styrene) (center) and poly(phenylene oxide) (right) as materials for AEM backbones⁷.

Several works have studied comparative stability with different backbones. Poly(sulfone)s contain strong electron withdrawing groups that promote nucleophilic attack and cause chain scission⁸. On the contrary, PS and PPO do not contain electron withdrawing groups and present better potential as backbones for AEM. Between these two different materials, PPO is usually chosen as the polymeric backbone of AEMFC because it consists of a hydrophobic polymer with great mechanical strength and high glass transition temperature ($T_g = 210\text{ }^\circ\text{C}$)⁹. Moreover, it is possible to synthetically modify its structure in various different sites to provide the desired charge densities for ion conduction.

Cationic groups

Among the various cationic groups considered for AEM are trimethyl ammonium (TMA), trimethyl phosphonium (TMP) and dimethyl sulfonium groups (DMS). The cationic groups are usually tethered to the backbone via single carbon chains, shown as R₁ and R₂ in Figure 2-3.

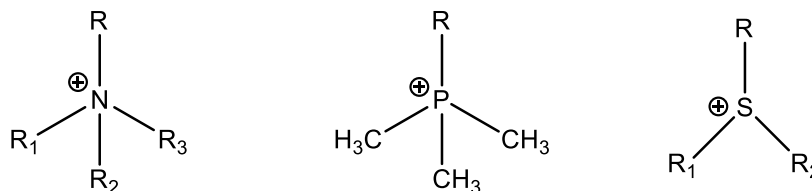


Figure 2-3. Ammonium (left), phosphonium (center) and sulfonium (right) groups as cationic groups for AEM¹⁰.

In this work¹⁰, Arges studied the stability of PSF functionalized membranes with different cations, including TMA and TMP. He subjected said membranes to degradation in 1 M KOH at 60°C and his results showed greater alkaline stability of TMA in comparison with TMP, as can be seen in Figure 2-4.

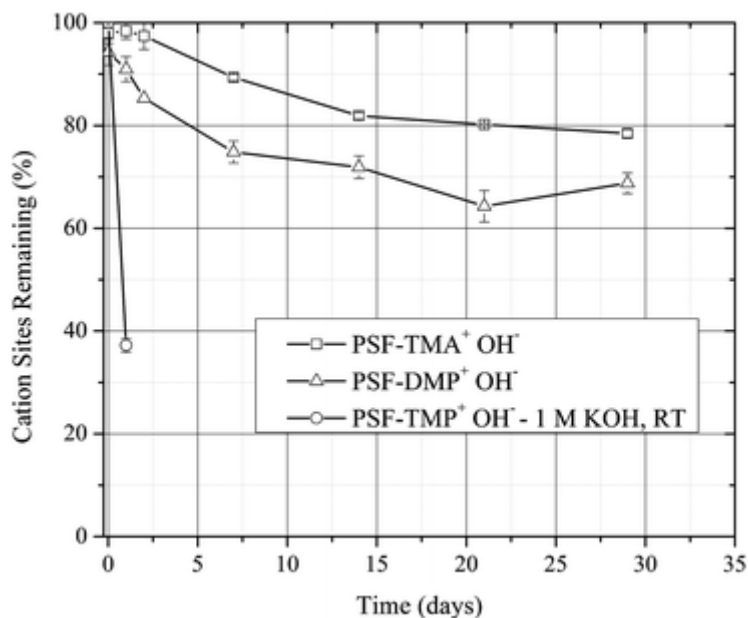


Figure 2-4. Alkaline stability of different cations functionalized to PSF at 1 M KOH, 60°C¹⁰.

The imidazolium group (Figure 2-5) is also usually considered as a candidate AEM cationic group. Many studies have shown high alkaline stability for the imidazolium group^{11,12}; however, in a study performed by Varcoe¹³ there is profound evidence that the imidazolium group presents relatively less thermochemical stability than the benchmark BTMA.

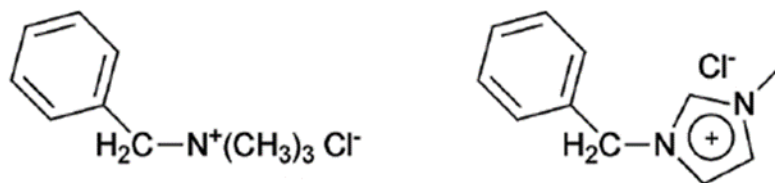


Figure 2-5. Study on relative stability of benzyltrimethylammonium chloride (left) and 1-benzyl-3-methylimidazolium (right) performed by Varcoe et al¹³.

In this study, chemical stability was measured by FT-Raman spectroscopy and analyzed in conjunction with other techniques such as ion exchange capacity (IEC) measurements, water uptake, ionic conductivity and fuel cell test data to provide an in-depth profile of the performance of such ions. A simple experiment performed in this study is shown below, where both ions were subjected to a heat treatment at 60°C in deionized water and aqueous KOH (1 M) for 14 days. A decrease in the intensity of the imidazolium-related bands (1025 cm⁻¹ and 1300-1500 cm⁻¹ range) suggests lower stability on the alkali treatment (Figure 2-6).

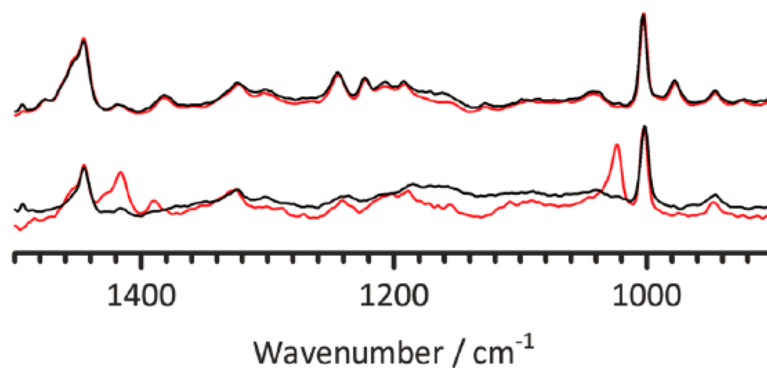


Figure 2-6. FT-Raman spectra of 1-benzyl-3-methylimidazolium chloride (bottom) and benzyltrimethylammonium chloride (top) after 14 days in heat treatment reveals decrease intensity in the imidazolium-related bands¹³.

It is worth mentioning that in this study, Varcoe reveals the importance of analyzing the stability of the cationic groups by utilizing a combination of chromatography/mass-spec data analysis with other techniques, such as IEC or ionic conductivity to fully understand the degradation of cationic groups in an alkaline environment. This thesis focuses on this approach.

From the different literature references shown above, it can be distinguished that there is no sustainable evidence on cations with significantly higher stability than benzyltrimethyl ammonium groups. This work will focus on strategies to increase the stability of quaternary-ammonium-based cations.

Stability of Anion Exchange Membranes

As it was mentioned before, stability of AEMs depends on both the stability of the backbone and the cationic group. Some studies even show evidence that polymer backbone degradation can be triggered by the added cationic group¹⁴. In consequence, the challenge is to find anion-exchange head groups with high stabilities and excellent conductivities. It was also stated that BTMA is the leader cation for AEM. It is the focus of this work to explore methods for achieving better cation stability and to understand the underlying degradation mechanisms.

Degradation mechanisms

The mechanisms by which the cationic group is attacked by hydroxide depend on the chemical composition of the membrane. The BTMA cation (Figure 2-3) has an electrophilic character, and is prone to attack by the nucleophilic OH^- that is present in the environment of the anion exchange membrane fuel cell. Several mechanisms can take place, as stated before, according to the chemistry of the cation.

In a nucleophilic substitution, a nucleophile replaces a leaving group from the electrophile using its lone pair of electrons to form a new bond. A general reaction for this mechanism is shown in Figure 2-7. Specifically, a nucleophilic substitution is called S_N2 when the rate limiting step involves the collision of two molecules, and S_N1 when there is only one molecule involved in the transition state of the rate limiting step.

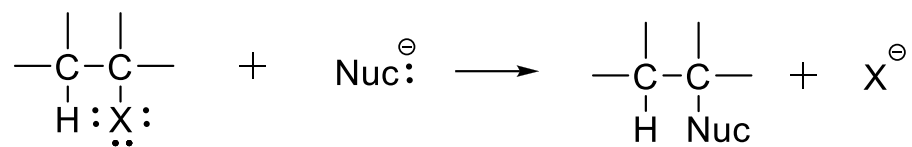


Figure 2-7. Nucleophilic substitution mechanism.

Usually competing with substitution reactions are elimination reactions, which involve the loss of two atoms or groups from the substrate, usually with the formation of a π bond. These reactions are usually called E_2 because they are second order transitions in which the nucleophiles attack the alkyl halide faster than it ionizes to give a first order reaction. An overall reaction for a general E_2 mechanism, also known as Hofmann elimination, is shown in Figure 2-8.

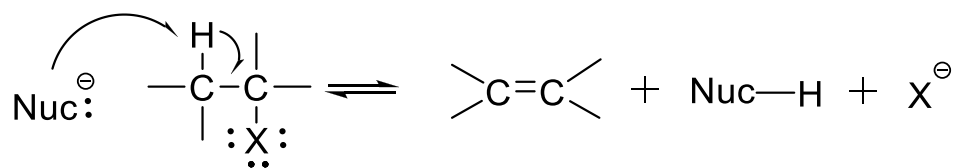


Figure 2-8. Elimination mechanism.

BTMA cations have two different hydrogens atoms that can be attacked by the OH^- and undergo degradation by a substitution reaction. Both hydrogens are located in the α position to the nitrogen; however, they can be differentiated by being in the methyl groups or in the benzyl

position. For the first one, the OH^- approaches the methyl group in which the carbon has a partial positive charge. The electrons in the carbon-nitrogen bond then migrate to the nitrogen, stabilizing the *benzyl dimethylamine*, and allowing the OH^- to form a new bond with the carbon and giving *methanol* as a product (Figure 2-9). This reaction is known as a *dealkylation* reaction due to the loss of the methyl group of the BTMA.

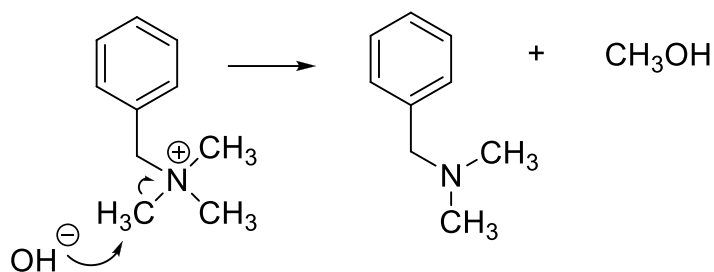


Figure 2-9. Dealkylation mechanism.

Opposite to the previous mechanism, the OH^- can also attack the carbon in the benzyl position. The mechanism is similar: the carbon-nitrogen electrons stabilize the *trimethylamine* while the OH^- forms a new bond with the benzene, giving as a product the *benzyl alcohol* (Figure 2-10). This reaction will be referred to as *substitution*.

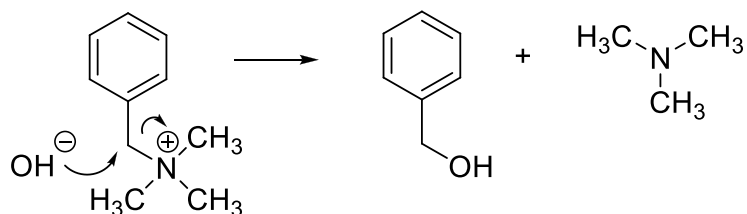


Figure 2-10. Substitution mechanism.

In the case of BTMA, Hofmann elimination cannot take place because of the lack of β -hydrogens (see Figure 2-11). However, when the design of the cation changes and β -hydrogens are introduced, this mechanism begins to take place and distinct degradation by-products are obtained. This is illustrated with a cation with an elongated alkyl chain between the benzyl group and the quaternary ammonium, *benzylpropyltrimethylammonium*, in Figure 2-11.

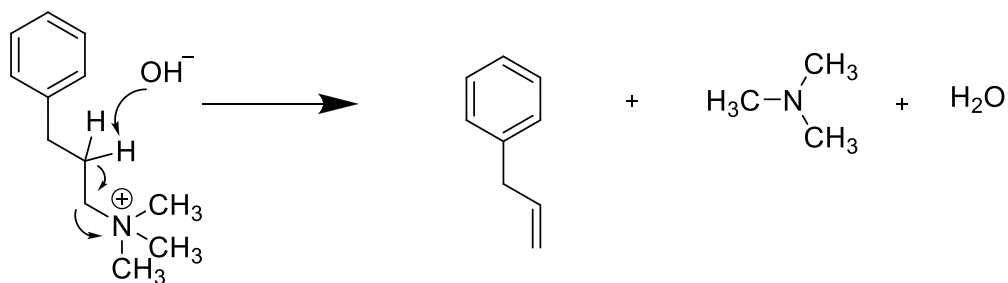


Figure 2-11. Hofmann elimination mechanism.

In this reaction, the OH^- approaches the β -hydrogen to the nitrogen, which donates its electrons to form a π bond between the α and β carbons, giving as a result *benzyl propene*, and forms a molecule of water. The α carbon then gives its two extra electrons to the electron-deficient nitrogen, which leaves as a stable *trimethylamine*.

Additionally, other degradation mechanisms can also be predicted to occur, depending on the structure of the cation, including Sommelet-Hauser and Stevens rearrangements¹⁵, and anion-induced 1,4-elimination¹³. However, these mechanisms have not been widely observed in either membrane or cation degradations¹⁶ and will not be considered for this work.

The three most important degradation mechanisms mentioned before have distinct by-products, thus, it is possible to identify which mechanism takes place if the degradation by-product is identified. This strategy is the one used throughout the course of this work to characterize the degradation mechanisms for each of the samples.

Alkyl spacers for enhanced stability

As was explained in the previous section, the presence of electron withdrawing groups like $-\text{CN}$ allows for the occurrence of degradation mechanisms. In a recent paper¹⁷, Kreuer claimed that “approaches to stabilize the amine via charge delocalization may not have been successful as they trade increased stability through delocalization with reduced stability from dramatically reduced steric shielding” and that the most promising approach towards QA stabilization is through the use of alkyl spacers to introduce a high degree of steric shielding. In fact, when the nucleophile approaches the back side of the electrophilic carbon atom, it must come within bonding distance of the back lobe of the C-N sp^3 orbital. If the carbon atom is crowded by the presence of bulky groups, this process is difficult and the rate of reaction is expected to be significantly lower¹⁸.

Strategies to suppress the reactive benzyl carbon were attempted by Hatch and Lloyd of Dow Chemical in anion exchange resins¹⁹, by substituting the benzyl hydrogens in a *benzyltrimethylammonium* resin for methyl groups, thus creating a resin with neither benzylic carbons nor β -hydrogens, which was expected to show improved stability compared with the common resins with benzyl groups. However, this resin lost strong base capacity more rapidly than the later ones. For the benzylic resins, about 60% of the breakdown would occur at the benzyl carbon. The authors hypothesized that the neophyl group in the *neophylbenzyltrimethylammonium* resin somehow caused the methyl carbons to be more susceptible to $\text{S}_{\text{N}}2$ attack.

Alkyl spacers between the aromatic ring and the cation - or spacer chains - were initially introduced by Tomoi in 1996²⁰. In this work, Tomoi synthesized various anion exchange resins with different lengths of carbon spacers to examine their relative stability (Figure 2-12 and Table 2-1).

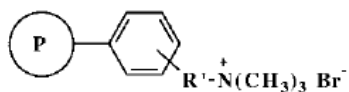
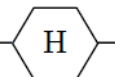


Figure 2-12. Anion exchange resins. R' indicates spacer chains²⁰.

Table 2-1. Spacer chains utilized for the anion exchange resins²⁰.

Spacer Chain ^a (R')
(CH ₂) ₄ CH ₂ CH ₂ CH(CH ₃)CH ₂
(CH ₂) ₃ CH(CH ₃)CH ₂ CH ₂ (CH ₂) ₇
CH ₂ CH ₂ —  —CH ₂
CH ₂ O(CH ₂) ₃
CH ₂ O(CH ₂) ₄
CH ₂ O(CH ₂) ₆

The thermal stability of said resins was examined by immersion in deionized water at 100-140 °C for 30 to 90 days and the stability was measured as a comparison of the strong base capacity of the resin after and before the temperature treatment. The study concluded that the introduction of alkyl – or alkyleneoxymethylene – spacers between the benzyl ring and the quaternary nitrogen improved the thermal stability of the resins (Figure 2-13).

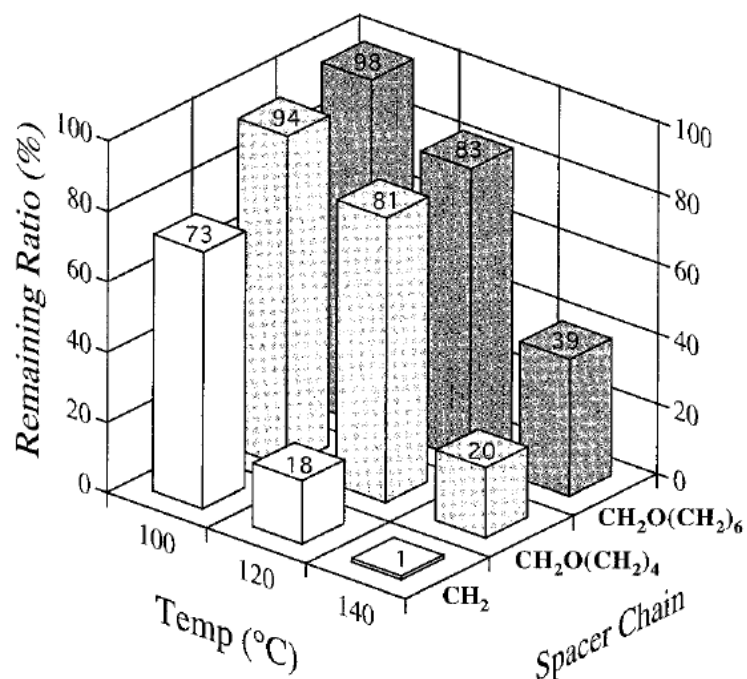


Figure 2-13. Thermal stability of alkyleneoxymethylene spacer-modified anion exchangers²⁰.

Interestingly, however, the material with the *propyleneoxymethylene* spacer showed less stability than the one with a single $-\text{CH}_2$ tethering, which could be explained by an additional electron-withdrawing effect of the *propylene* group, which increased the reactivity of the β -carbon. Consequently, the authors argued that enhanced stability can be achieved for resins with alkyl spacers longer than the propylene chain and that the main decomposition in anion exchangers containing spacer chains would be likely to occur at the methylene or methyl carbon.

Additionally, this strategy was further investigated by Hibbs by comparing the stability of poly(phenylene)-based AEMs containing (i) a single tethered *trimethylammonium* (ATMPP) and (ii) an *hexane-1-one-6-trimethylammonium* (TMAC6PP)²¹. The stability was tested by exposing membrane samples to 4 M KOH at 90°C for 14 days and comparing both Cl^- conductivity and ion exchange capacity. Other samples studied include a resonance-stabilized benzyl

pentamethylguanidinium (PMGTMPP), an imidazolium-based poly(phenylene) (ImTPP) and a sidechain ketone (TMAKC6PP) (Figure 2-14 and Figure 2-15).

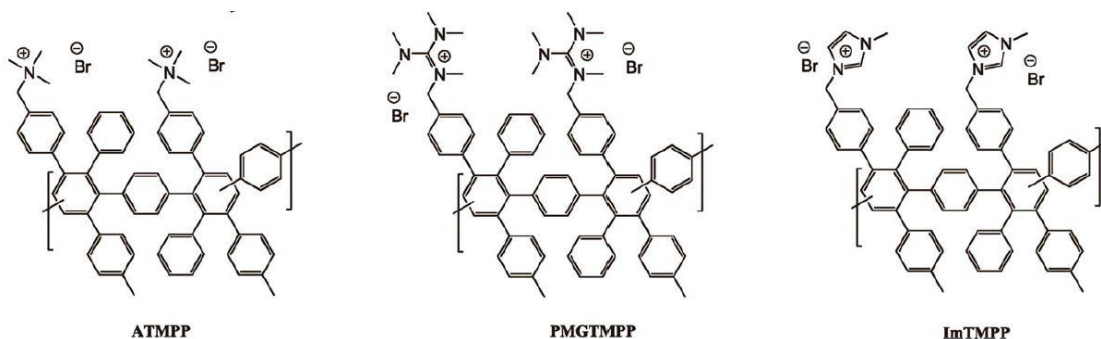


Figure 2-14. Poly(phenylene)s with benzylic cations studied by Hibbs²¹.

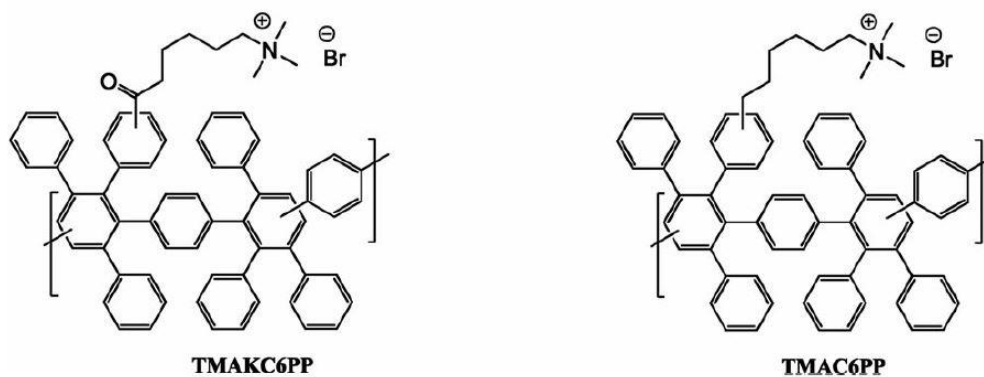


Figure 2-15. Poly(phenylene)s with sidechain tethered cations studied by Hibbs²¹.

Figure 2-16 shows the change in Cl^- conductivity during the temperature test for the different cations. The open triangle (TMAC6PP) and filled circle (ATMPP) show the greatest stability, with a comparatively greater stability of the spacer-modified cation.

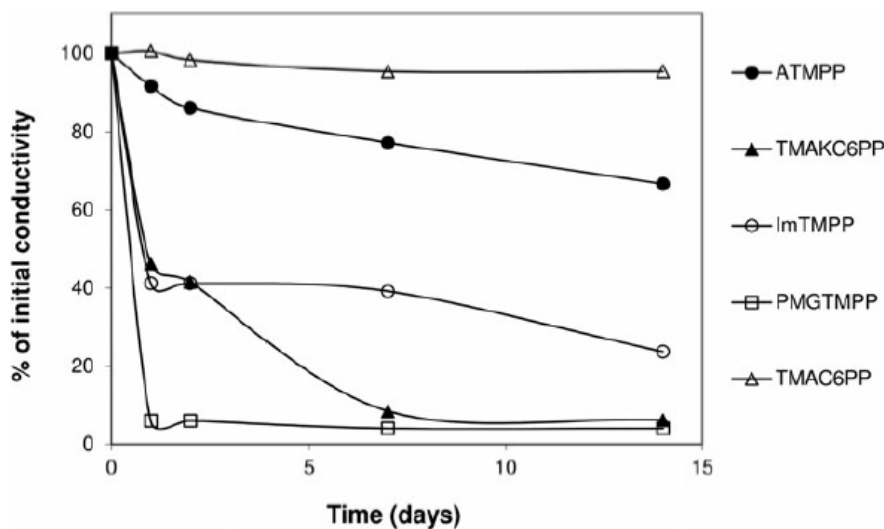


Figure 2-16. Changes in chloride ion conductivity during test in 4 M KOH at 90°C²¹.

Pendant chains

Another strategy towards gaining exceptional stability is the incorporation of pendant chains to the cationic center. This approach also focuses on creating steric hindrance around the electrophilic carbons to lower the rate of the reaction. A series of quaternized PPOs containing long pendant chains of 6, 10 and 16 carbons were synthesized by Li and their hydroxide conductivity and ion exchange capacity were measured to determine their relative stability²². The hexadecyl pendant chain with 40% functionalization showed the best properties, including higher hydroxide conductivity although its lower IEC value; however, the inability to form films made this polymer not suitable for membrane capabilities. The membranes containing a hexyl chain showed great potential for highly stable AEMs, as it can be seen from the plots of conductivity as a function of IEC and IEC over time (Figure 2-17).

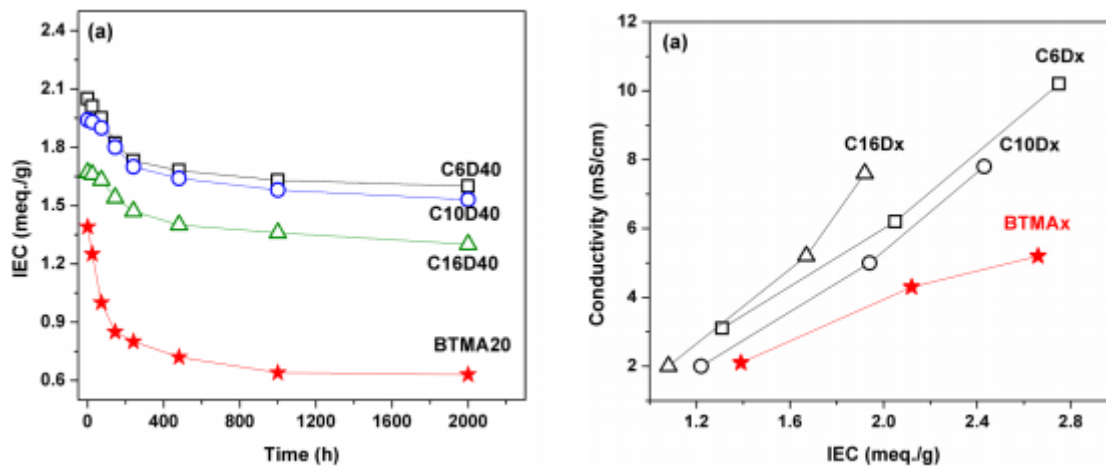


Figure 2-17. Hydroxide conductivity at 20°C as a function of ion exchange capacity (left) and changing trend in IEC values after immersion in 1 M NaOH at 80°C²².

This study concluded that “the steric effects of the long alkyl chains surrounding the quaternary ammonium center are likely the cause of these materials’ good alkaline stability”.

Nuclear Magnetic Resonance (NMR)

NMR is one of the most powerful tools available for determining organic structures. The NMR spectrum provides great information about the structure of the sample, and it is sometimes used with other spectroscopy techniques to determine the structures of complicated organic molecules. A wide variety of nuclei are studied by NMR, being proton (^1H) and carbon-13 (^{13}C) the most useful because they are the major components of organic compounds¹⁸.

Theory of Nuclear Magnetic Resonance

A nucleus with an odd atomic number or an odd atomic mass, like hydrogen, has a nuclear spin and the number of allowed spin states it may adopt is quantized and determined by

its spin nuclear quantum number I . The spin angular momentum generates a magnetic field B , also called the magnetic moment. When the proton is placed in an external magnetic field, it can re-orient with or against it. The lower energy state of the proton is with its spin aligned with the external field, and the energy difference between the low and high state is quantized and proportional to the field²³. When a nucleus is subjected to the exact combination of magnetic field and electromagnetic radiation to flip its spin, it becomes in resonance with the field, and the absorption of energy can be detected by the NMR. This is the reason to call it “nuclear magnetic resonance”. However, electrons that circulate create a small induced magnetic field opposite to the applied external field, which generates a “shield” around the proton and in consequence, the magnetic field at the nucleus is weaker than the external field, so the applied field must be increased for resonance to occur. The way a proton is surrounded by a chemical environment changes the difference between the magnetic field at the nucleus and the external one, giving each proton a characteristic energy difference to be absorbed to gain resonance, also called chemical shifts. Chemical shifts are recorded in a spectrum against a reference proton, and the relative positions of the chemical shifts are unique to specific protons. An example of ethyl acetate is shown in Figure 2-18.

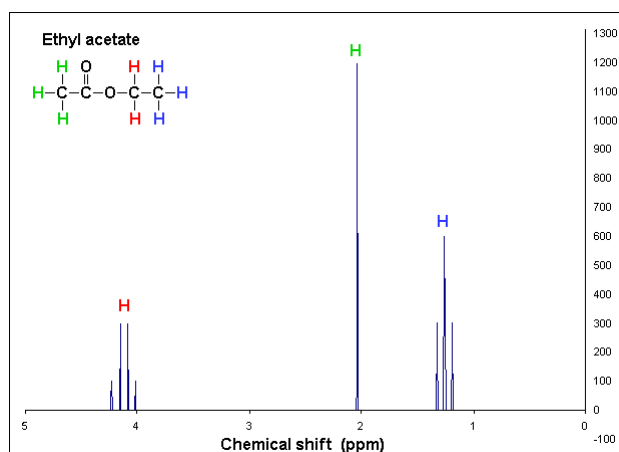


Figure 2-18. ^1H NMR spectrum of ethyl acetate, intensity versus chemical shift.

^1H NMR and stability of AEMs

The versatility of ^1H NMR has made it a powerful tool that has been widely used to study AEMs, mainly to confirm synthesized polymers and membranes²⁴; however, this spectroscopy technique has various applications and was also reported to be used as a comparative technique for relative stability²⁵, and to determine degradation profiles²⁶. An example of the first approach is shown in Figure 2-19, where an imidazolium-based alkaline anion exchange membrane was subjected to a stability test of oscillating relative humidity (RH) at 30 °C. No major changes in the spectrum before and after the test suggested the sample's chemical stability.

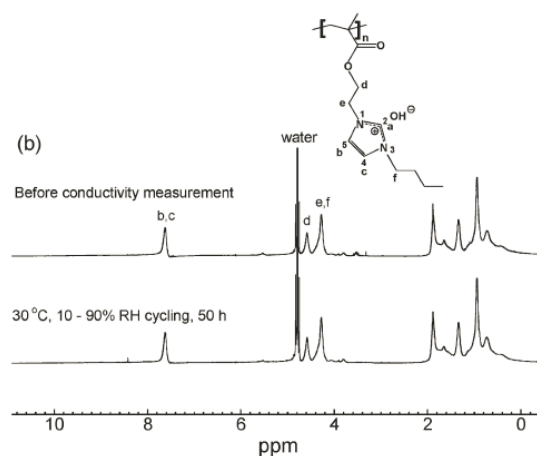


Figure 2-19. Comparison of ^1H NMR spectra of an imidazolium-based membrane before and after stability test²⁵.

As mentioned before, NMR has also been used to develop degradation profiles of desired samples. Figure 2-20 shows the degradation profile of two small molecule imidazolium salts in a solution of 1 M NaOH in 4:1 $\text{D}_2\text{O}:\text{CD}_3\text{OD}$ at 60°C over the course of 48 hours. The appearance of new peaks in the region of 6.5-7.0 ppm suggest a greater instability of compound *a* compared to compound *b*, the later which was designed with more bulky groups around the cation site.

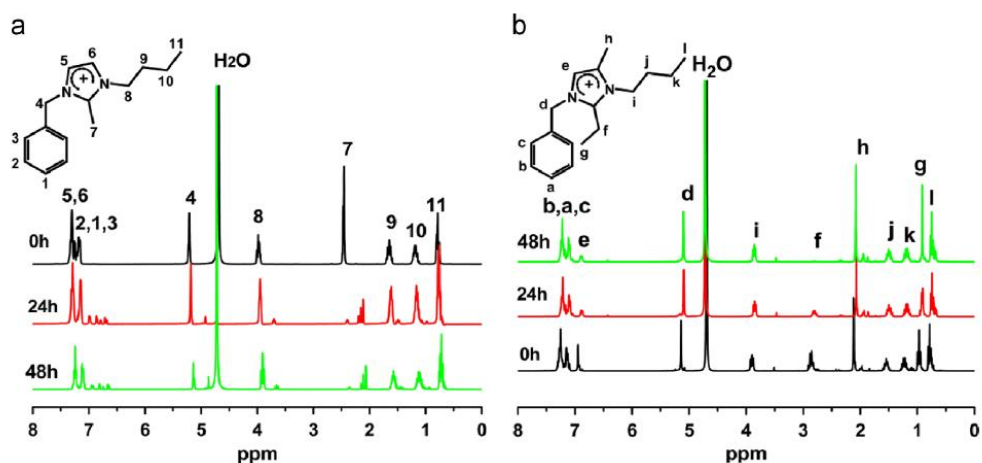


Figure 2-20. Degradation profile from ^1H NMR spectra for small molecule imidazolium salts in 1 M NaOH in 4:1 $\text{D}_2\text{O}:\text{CD}_3\text{OD}$ at 60°C for 48 hours²⁵.

Liquid Chromatography Mass Spectrometry

Liquid chromatography and mass spectrometry are two very important analytical techniques that combined provide a great deal of information about a sample. The chromatography portion is a physical method of separation in which components of different characteristics are distributed between two phases²⁷. The mass spectrometer will then generate ions for either the organic or inorganic compounds by any suitable method, such as electric fields or energetic electrons, separate the ions according to their mass-to-charge ratio (m/z) and detect them both quantitatively and qualitatively by their respective m/z abundance²⁸. The two techniques combined are able to separate distinct components of a sample and identify their different m/z , which can be further translated into molecular weight.

Liquid Chromatography

As it was explained before, chromatography is a physical method of separating components which are distributed in two phases, one that does not move (stationary phase) and another one that moves in a definite direction (mobile phase)²⁸. In liquid chromatography (LC), the sample is passed through a column at a finite rate. Once the sample has been injected, it starts to flow through the column, where a partial separation begins. The separation improves as the sample moves further through the column until the distinct components are essentially separated from each other and elute at different times. The distribution and separation of the different components is both related to the identity of the column and the chosen solvents. The strength of the sample's interaction with the mobile and stationary phase determines the rate of retention in LC. An appropriate solvent should have low viscosity, be compatible with the detection system, be easily available with high purity, and have low flammability and toxicity. Common LC

solvents are water, acetonitrile and methanol. Additionally, it is sometimes necessary to add additives such as acetic acid to improve selectivity, reproducibility and peak shape.

It is estimated that approximately 65% of all LC separations are executed in the reverse-phase mode; this is, on columns where the stationary phase surface is less polar than the mobile phase. The universality of reversed-phase LC arises from the fact that organic molecules have hydrophobic regions that interact effectively with the stationary phase. Columns used for reversed-phase LC usually possess a ligand such as octadecyl (C-18) chemically bonded to microporous silica particles²⁹.

Mass Spectrometry

Mass spectrometry (MS) is a technique in which a sample is ionized, separated according to their mass-to-charge ratio (m/z) and then detected and recorded. The instrument is called a mass spectrometer and it is a destructive technique since the sample is ionized³⁰. The mass spectrometer usually consists of five components: the sample inlet, an ion source, the mass analyzer, the detector and the data system (Figure 2-21). In the inlet, the sample is pressurized and transported to the ion source, where it is transformed into gas phase ions. There are different ionization techniques, including electron ionization, fast atom bombardment, chemical ionization and electrospray ionization. Once the sample is ionized, it is accelerated by an electromagnetic field. The mass analyzer separates the ion based on their m/z ratio and the detector then counts the ions. The signal is recorded and processed by the data system and the information is given in a mass spectrum, a graph of the number of ions detected (or abundance) as a function of their m/z ratio³¹.

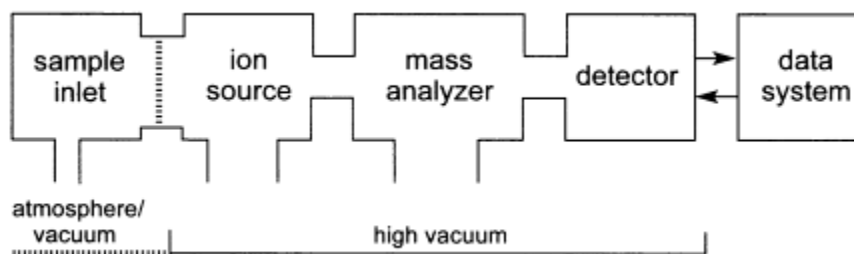


Figure 2-21. General scheme of a mass spectrometer.

One of the most commonly used ionization techniques is electrospray ionization, and it is also the method of choice for LC-MS. It is a soft ionization technique and it has extraordinary high-mass capability²⁷.

LC-MS in polymer degradation

Understanding the degradation mechanisms and by-product distribution of AEMs in fuel cell working conditions allows for the re-design of the membranes' chemistry to achieve greater stability. The most common approach towards analyzing AEMs stability has been to compare properties such as ion exchange capacity^{32,33}, conductivity and mechanical properties before and after certain degradation tests. However, little information of the degradation mechanisms can be obtained with said approaches. LC-MS has the advantage of being able to separate the degradation by-products, thus understanding the degradation mechanisms.

In a study previously mentioned²⁶, mass spectrometry was used to confirm the suspected degradation by-products of a cation for potential AEMs after a degradation procedure. The sample in question, a small molecule imidazolium salt (Figure 2-22), was degraded in 1 M NaOH at 60°C for 48 hours.

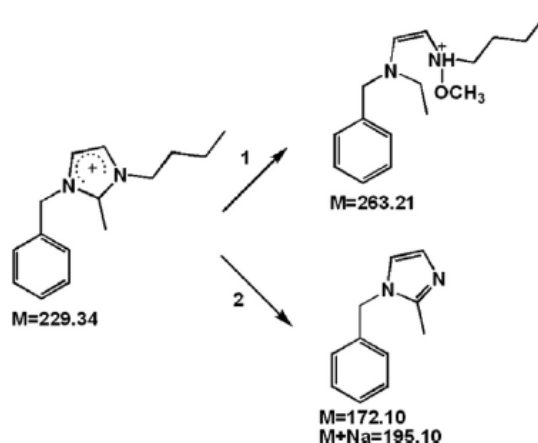


Figure 2-22. Degradation pathways of the small molecule imidazolium salt²⁵.

The sample was also studied by LC-MS (Figure 2-23). The peak of m/z 229.2 is assigned to the model compound, and two degradation by-products were observed (m/z 263.2 and m/z 195.1), the alcoholysis and dealkylation mechanisms products respectively.

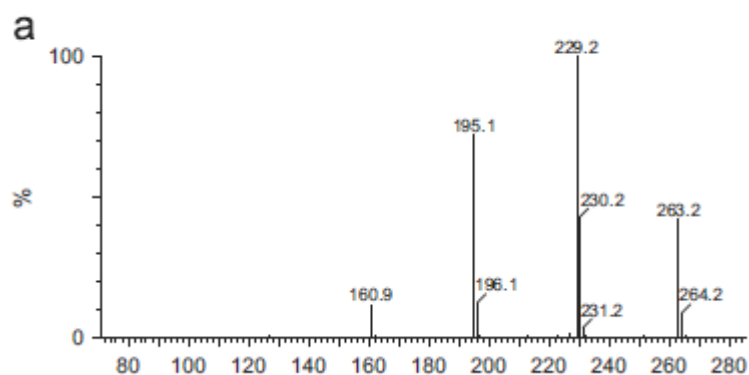


Figure 2-23. MS of the model compound after the alkaline stability test²⁵.

LC-MS was also used to identify the chain end unzipping degradation mechanism in Nafion and related perfluoro sulfonic acid model compounds³⁴. This mechanism was verified by the analysis of a molecule containing a carboxylic group on a linear perfluorinated aliphatic chain

(R_f-COOH). A full chromatograph showed a series of peaks at different elution times (Figure 2-24, top). Specific ion molecular weights were extracted from the full chromatograph to show the relative intensity of those specific ions at different elution times (Figure 2-24). This becomes an extracted chromatograph. The difference between the six deconvoluted peaks arise from the loss of a -CF₂- unit (50 Da.), which is consistent with the unzipping degradation mechanism.

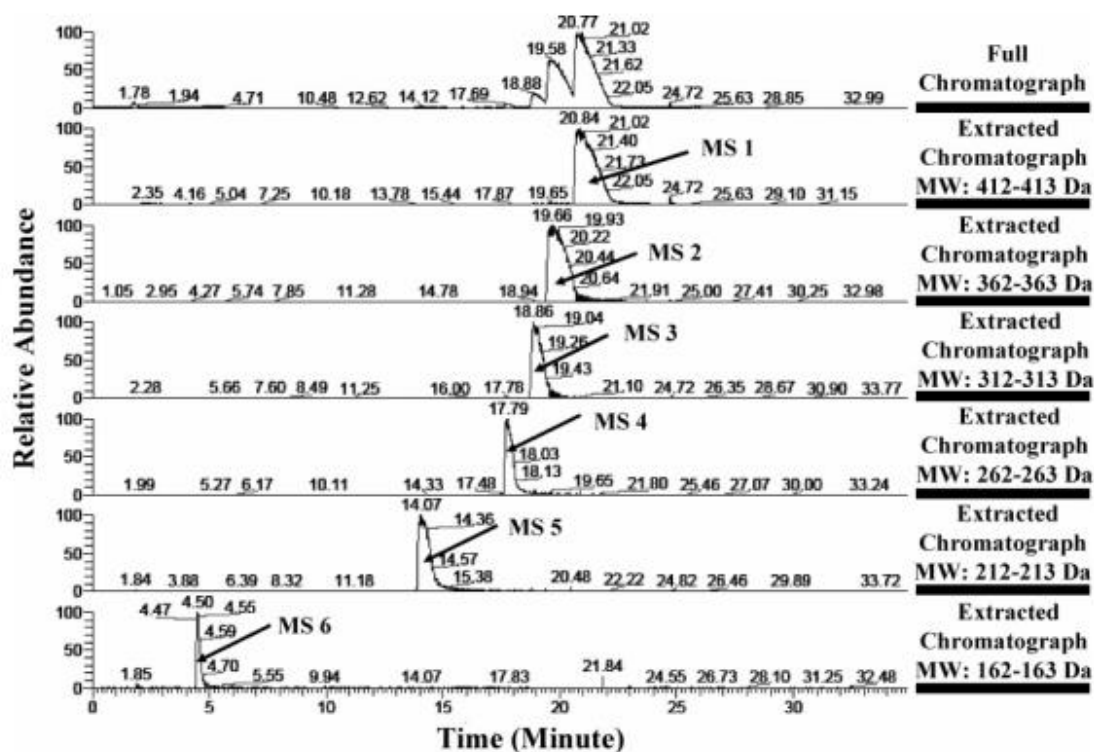


Figure 2-24. LC chromatographic trace of degraded model compound³⁴.

The MS spectrums of each peak in Figure 2-24 were recorded as shown in Figure 2-25.

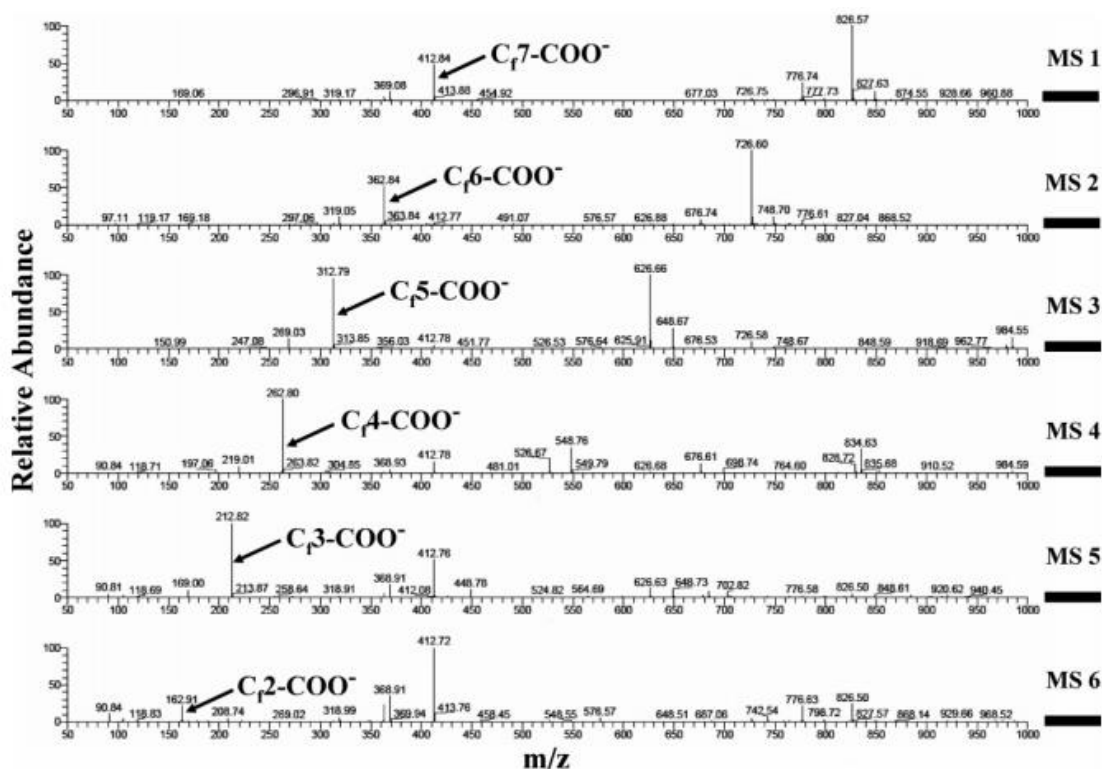


Figure 2-25. MS spectra of LC trace of degraded model compound product mixture at different elution times³⁴.

Summary

This chapter has explained the fundamentals of fuel cells and the need of more stable AEMs. Examples of both polymeric backbones and cationic groups were exposed and the most stable cationic group was presented. Additionally, the degradation mechanisms were explained and strategies to achieve more stable AEMs were introduced, along with examples of previous work in the area. Moreover, the techniques and equipment used for this work were exhibited for some understanding of the advantages they present.

1. Carrette, L., Friedrich, K. A., & Stimming, U. (2001). Fuel cells—fundamentals and applications. *Fuel cells*, 1(1), 5-39.
2. Varcoe, J. R., Atanassov, P., Dekel, D. R., Herring, A. M., Hickner, M. A., Kohl, P. A., ... & Zhuang, L. (2014). Anion-exchange membranes in electrochemical energy systems. *Energy & Environmental Science*, 7(10), 3135-3191.
3. Adams, L. A., Poynton, S. D., Tamain, C., Slade, R. C., & Varcoe, J. R. (2008). A Carbon Dioxide Tolerant Aqueous-Electrolyte-Free Anion-Exchange Membrane Alkaline Fuel Cell. *ChemSusChem*, 1(1-2), 79-81.
4. Shaji Chempath, James M. Boncella, Lawrence R. Pratt, Neil Henson, and Bryan S. Pivovar, Density Functional Theory Study of Degradation of Tetraalkylammonium Hydroxides, *The Journal of Physical Chemistry C* 2010 114 (27), 11977-11983
5. Yan, J., & Hickner, M. A. (2010). Anion exchange membranes by bromination of benzylmethyl-containing poly (sulfone)s. *Macromolecules*, 43(5), 2349-2356.
6. Hickner, M. A., Herring, A. M., & Coughlin, E. B. (2013). Anion exchange membranes: current status and moving forward. *Journal of Polymer Science Part B: Polymer Physics*, 51(24), 1727-1735.
7. Nuñez, S. A.; Hickner, M. A. Quantitative ¹H NMR Analysis of Chemical Stabilities in Anion-Exchange Membranes. *ACS Macro Lett.* 2013, 2, 49–52.
8. Arges, C. G., Parrondo, J., Johnson, G., Nadhan, A., & Ramani, V. (2012). Assessing the influence of different cation chemistries on ionic conductivity and alkaline stability of anion exchange membranes. *Journal of Materials Chemistry*, 22(9), 3733-3744.
9. Xu, T., Wu, D., & Wu, L. (2008). Poly (2, 6-dimethyl-1, 4-phenylene oxide)(PPO)—a versatile starting polymer for proton conductive membranes (PCMs). *Progress in Polymer Science*, 33(9), 894-915.
10. Arges, C. G., Parrondo, J., Johnson, G., Nadhan, A., & Ramani, V. (2012). Assessing the influence of different cation chemistries on ionic conductivity and alkaline stability of anion exchange membranes. *Journal of Materials Chemistry*, 22(9), 3733-3744.
11. Qiu, B., Lin, B., Qiu, L., & Yan, F. (2012). Alkaline imidazolium-and quaternary ammonium-functionalized anion exchange membranes for alkaline fuel cell applications. *Journal of Materials Chemistry*, 22(3), 1040-1045.
12. Li, W., Fang, J., Lv, M., Chen, C., Chi, X., Yang, Y., & Zhang, Y. (2011). Novel anion exchange membranes based on polymerizable imidazolium salt for alkaline fuel cell applications. *Journal of Materials Chemistry*, 21(30), 11340-11346.
13. Deavin, O. I., Murphy, S., Ong, A. L., Poynton, S. D., Zeng, R., Herman, H., & Varcoe, J. R. (2012). Anion-exchange membranes for alkaline polymer electrolyte fuel cells: comparison of pendent benzyltrimethylammonium-and benzylmethylimidazolium-head-groups. *Energy & Environmental Science*, 5(9), 8584-8597.
14. Arges, C. G., & Ramani, V. (2013). Two-dimensional NMR spectroscopy reveals cation-triggered backbone degradation in polysulfone-based anion exchange membranes. *Proceedings of the National Academy of Sciences*, 110(7), 2490-2495.
15. Arges, C. G., & Ramani, V. (2013). Investigation of cation degradation in anion exchange membranes using multi-dimensional NMR spectroscopy. *Journal of The Electrochemical Society*, 160(9), F1006-F1021.
16. Nuñez, S. A.; Capparelli, C; Hickner, M. A. N-Alkyl Interstitial Spacers and Terminal Pendants Influence on the Alkaline Stability of Tetraalkylammonium Cations for Anion Exchange Membrane Fuel Cells. Submitted.
17. Kreuer, K. D. (2013). Ion conducting membranes for fuel cells and other electrochemical devices. *Chemistry of Materials*, 26(1), 361-380.
18. Wade, L. J. Jr. (2006). *Organic chemistry*, Sixth edition. Pearson.
19. Hatch, M. J., & Lloyd, W. D. (1964). Preparation and properties of a neophyl type anion exchange resin. *Journal of Applied Polymer Science*, 8(4), 1659-1666.
20. Tomoi, M.; Yamaguchi, K.; Ando, R.; Kantake, Y.; Aosaki, Y.; Kubota, H. Synthesis and Thermal Stability of Novel Anion Exchange Resins with Spacer Chains. *Journal of Applied Polymer Science* 1997, 64, 1161–1167.

-
21. Hibbs, M. R. (2013). Alkaline stability of poly (phenylene)-based anion exchange membranes with various cations. *Journal of Polymer Science Part B: Polymer Physics*, 51(24), 1736-1742.
 22. Li, N., Leng, Y., Hickner, M. A., & Wang, C. Y. (2013). Highly stable, anion conductive, comb-shaped copolymers for alkaline fuel cells. *Journal of the American Chemical Society*, 135(27), 10124-10133.
 23. Pavia, D., Lampman, G., Kriz, G., & Vyvyan, J. (2008). *Introduction to spectroscopy*. Cengage Learning.
 24. Wang, J., Wang, J., Li, S., & Zhang, S. (2011). Poly(arylene ether sulfone)s ionomers with pendant quaternary ammonium groups for alkaline anion exchange membranes: preparation and stability issues. *Journal of Membrane Science*, 368(1), 246-253.
 25. Ye, Y., & Elabd, Y. A. (2011). Relative chemical stability of imidazolium-based alkaline anion exchange polymerized ionic liquids. *Macromolecules*, 44(21), 8494-8503.
 26. Yang, Y., Wang, J., Zheng, J., Li, S., & Zhang, S. (2014). A stable anion exchange membrane based on imidazolium salt for alkaline fuel cell. *Journal of Membrane Science*, 467, 48-55.
 27. Gross, J. H. (2004). *Mass spectrometry: a textbook*. Springer Science & Business Media.
 28. Ahuja, S. (2003). *Chromatography and separation science (Vol. 4)*. Academic Press.
 29. Meyer, V. R. (2013). *Practical high-performance liquid chromatography*. John Wiley & Sons.
 30. Barker, J. (1999). *Mass Spectrometry; Analytical Chemistry*. Open Learning.
 31. Pavia, D., Lampman, G., Kriz, G., & Vyvyan, J. (2008). *Introduction to spectroscopy*. Cengage Learning.
 32. Sata, T., Tsujimoto, M., Yamaguchi, T., & Matsusaki, K. (1996). Change of anion exchange membranes in an aqueous sodium hydroxide solution at high temperature. *Journal of membrane science*, 112(2), 161-170.
 33. Bauer, B., Strathmann, H., & Effenberger, F. (1990). Anion-exchange membranes with improved alkaline stability. *Desalination*, 79(2), 125-144.
 34. Zhou, C., Guerra, M. A., Qiu, Z. M., Zawodzinski, T. A., & Schiraldi, D. A. (2007). Chemical durability studies of perfluorinated sulfonic acid polymers and model compounds under mimic fuel cell conditions. *Macromolecules*, 40(24), 8695-8707.

Chapter 3

Experimental procedures for sample preparation and characterization

Introduction

This section will describe the details of sample preparation, degradation treatments and post-test characterization and analysis. The first section of the chapter will explain the procedure for the synthesis of all the samples used for this work. The second section will describe the degradation experiments performed on the samples and the last section will explain the methods and procedures used to analyze the samples after they were exposed to the degradation treatment. In this work, two characterization methods were employed for the analysis – ^1H Nuclear Magnetic Resonance (NMR) and Liquid Chromatography – Mass Spectrometry (LC-MS).

Synthesis of Small Molecule Cations as Analogues for AEM Degradation

Degradation of AEMs is being thoroughly investigated because of the interest in developing clean, renewable energy sources. However, it has been difficult for the scientific community to come to a consensus on the main degradation pathways of AEM because of (a) the different methodologies and experimental setups, which include concentration of OH^- and temperature¹, and (b) the fact that reactivity of AEMs depends on a variety of factors, including solvation, water uptake and chemical structure. As explained by Kreuer, the complexity of sorting out the degradation pathways in these materials can be lowered by studying analogue small molecule cations to obtain reliable conclusions². With undeniable precedents of this approach in the literature, small molecule cations were synthesized to serve as cases of study for AEMs.

In order to investigate the influence of alkyl spacers and pendant chains as means of stabilizing cations for AEMs, five different small molecule cations with distinctive chemistries were designed, as shown in Figure 3-1.

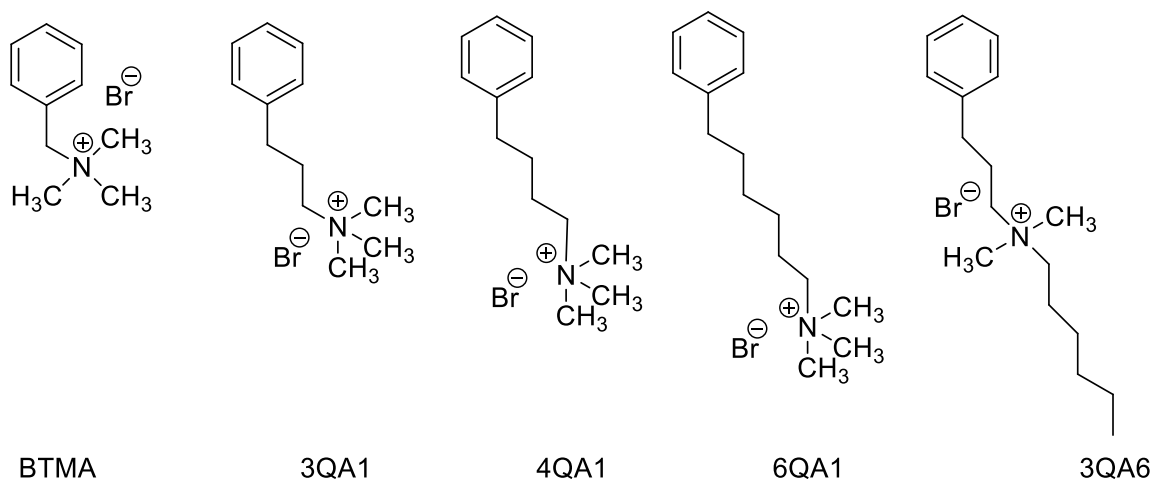


Figure 3-1. Small Molecule Cations synthesized for degradation experiment, from left to right, BTMA, 3QA1, 4QA1, 6QA1 and 3QA6 in their salt form.

Samples BTMA -1QA1 if following the same classification as the other samples, but will be called BTMA for simplification-, 3QA1, 4QA1, and 6QA1 exemplify the concept of alkyl spacers, introducing an extra methyl group when going from sample 3QA1 to 4QA1 and two extra methyl groups when going from samples BTMA ns 3QA1, and 4QA1 and 6QA1. Sample 3QA6 was designed to introduce the concept of pendant chain, as discussed in the literature review. In this sample, a pendant chain of six carbons was used in addition to an alkyl spacer consisting of three carbons.

Samples BTMA, 3QA1, 4QA1, and 6QA1 were all synthesized using the same synthetic route. The bromide versions of the samples were reacted with *trimethylamine* to form the QA, Figure 3-2.

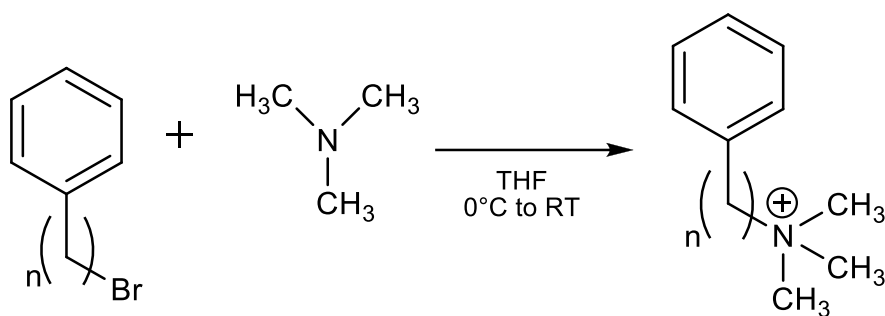


Figure 3-2. Synthetic route used for samples BTMA, 3QA1, 4QA1 and 6QA1, with n being 1, 3, 4 and 6 respectively.

The synthetic procedure was as following: an addition funnel was filled with one equivalent of the bromine compound dissolved in tetrahydrofuran (THF) (1.0 M). Subsequently, to a round bottom flask containing a stir bar was added the trimethylamine (10.0 equivalents) in THF (2.0 M). The round bottom flask was settled in a Dewar flask containing an ice bath. The sealed addition funnel was connected to the round bottom flask; the solution of the bromide compound was slowly added to the amine and left stirring overnight. After reaction was completed (versus TLC), the product was bubbled with nitrogen gas for about 3 hours to evaporate the remaining trimethylamine. The solvent was then removed under reduced pressure and the aqueous phase was removed by lyophilization. The final product was then washed with 45 mL of ethyl ether (3 x 15 mL), after which it was dry under vacuum overnight. Exact amounts and starting compounds for every sample are listed in Table 3-1.

Table 3-1. Exact amounts of starting materials for samples BTMA, 3QA1, 4QA1 and 6QA1.

	SAMPLE			
	BTMA	3QA1	4QA1	6QA1
Bromine compound	benzyl bromide 1.078 mL	1-bromo-3-phenylbutane 1.183 mL	1-bromo-4-phenylbutane 1.28 mL	1-bromo-6-phenylbutane 0.668 mL
Trimethylamine, 45% acq. sol.	14.37 mL	12.02 mL	11.5 mL	5.3 mL
THF (addition funnel)	9.1 mL	7.53 mL	7.3 mL	3.33 mL

THF (round bottom flask)	45.5 mL	38 mL	36.35 mL	16.5 mL
--------------------------	---------	-------	----------	---------

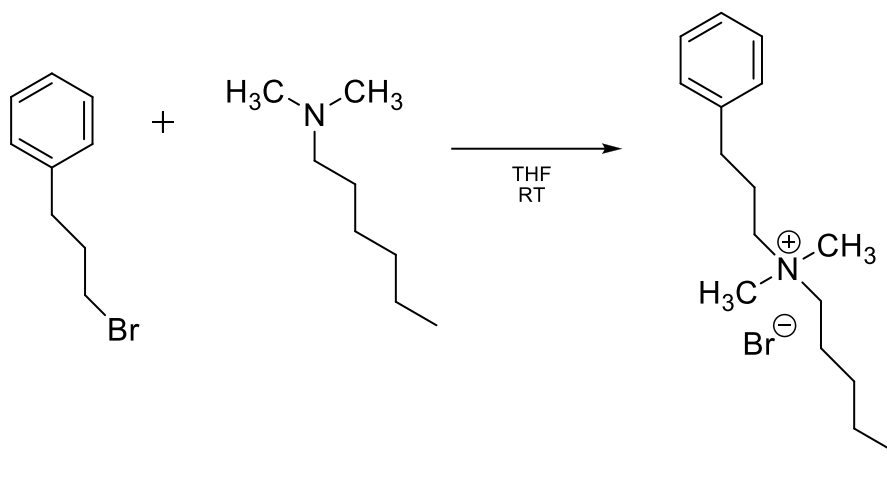


Figure 3-3. Synthetic route used for sample 3QA6.

Sample 3QA6 was synthesized in a similar fashion (Figure 3-3), using one equivalent of 1-bromo-3-phenylbutane and 2.2 equivalents of N,N-dimethylhexylamine as the starting materials (see Table 3-2. Starting materials for sample 3QA6). The reaction was performed at room temperature and left stirring overnight. The product was precipitated with hexanes, the precipitate was removed and redissolved in THF for a total of three times to eliminate all traces of solvent. The powder-looking final product was dried under vacuum overnight.

Table 3-2. Starting materials for sample 3QA6.

	3QA6
1-bromo-3-phenylbutane	1.183 mL
N,N-dimethylhexylamine, 98%	2.94 mL
THF (addition funnel)	7.53 mL
THF (round bottom flask)	8.3 mL

Degradation experiments

The small molecules were degraded in an environment with high hydroxide concentration at high temperature to accelerate degradation of these molecules. The samples were dissolved in a solution of water containing a previously fixated amount of base and an internal standard to account for the absolute rate of degradation. The solution was designed as containing 30 mM of the sample and the internal standard, with 20 equivalents of base³. The solution was made with deuterated solvents (D₂O, NaOD) in order to be properly measured by NMR. The internal standard chosen was 1,4-dioxane because of its inert properties, water miscibility and high boiling point (101.1°C). Table 3-3 summarizes the amounts of water, base and internal standard used for each sample.

Table 3-3. Experimental setup for each of the samples.

	SAMPLE				
	BMTA	3QA1	4QA1	6QA1	3QA6
Small molecule (g)	0.055	0.061	0.065	0.0598	0.06
D ₂ O (mL)	7.543	7.543	7.543	7.543	7.543
1,4-dioxane (μL)	120	120	120	120	120
NaOD (μL)	337	337	337	337	337

Poly(tetrafluoroethylene) (PTFE) vials were used for the degradation experiment because it was observed that glass vials showed glass leaching at the base concentration (0.6 M) and temperature used (120 °C). PTFE vials were tested for fluoride leaching prior to using them for the experiment. For the test, the vials were filled with a solution of 0.6 M of NaOH and were heated in an oven for over 48 hours at a temperature of 120 °C. A fluoride test (Sigma-Aldrich, Fluoride Test Kit Quantofix) was performed for the final solution, showing 0 mg/mL of fluoride in both cases (Figure 3-4).

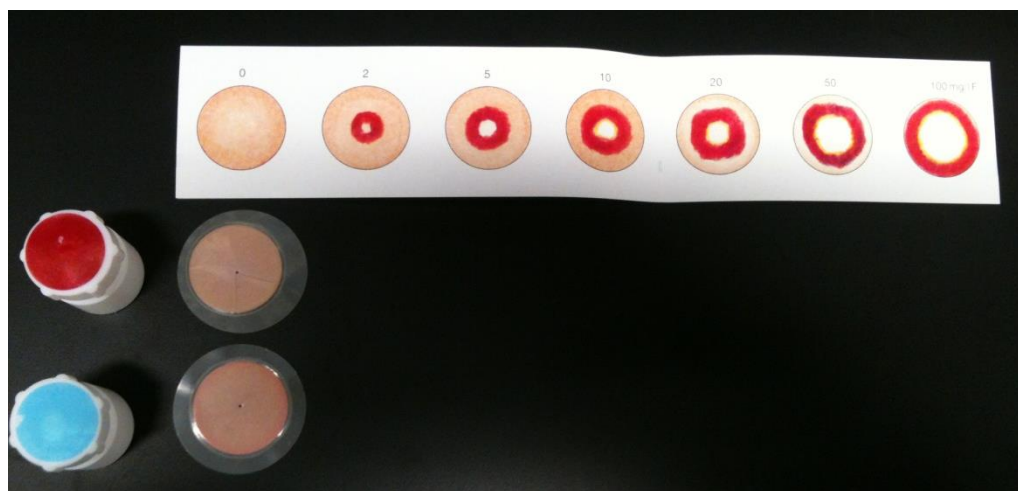


Figure 3-4. Fluoride test performed on the PTFE vials. Color scale shows test discs from 0 to 100 mg/L of F⁻. Comparison of discs used to analyze solution after degradation treatment reveals 0 mg/L of F⁻.

The samples were weighed and transferred to 20 mL PTFE vials, followed by the addition of the correspondent amount of D₂O, 1,4-dioxane and NaOD. An aliquot (approximately 0.8 mL) was taken at time zero and transferred to an NMR tube (Norell, 5 mm NMR Sample Tube). Additionally, an aliquot of 20 μ L was transferred to a 25 mL scintillation vial, previously filled with 10 mL of HPLC grade water (JT Baker). The scintillation vial was shaken thoroughly and 1.5 mL were transferred to a 1.5 mL autosampler vial. The PTFE vial was put in an oven previously heated at 120 °C. The same aliquots were taken at intervals of 1, 2, 3, 6, 9, 12, 24 and 48 hours, taking special care of cooling down the PTFE vial in a freezer for approximately 15-20 minutes prior to each extraction, to avoid the evaporation of solvents and internal standard.

Liquid Chromatography Mass Spectrometry Analysis

The LC-MS unit was equipped with an autosampler, MS pump, UV detector and MS detector. The Surveyor Autosampler Plus from Thermo Electron Corporation was able to hold up to 400 conventional vials. The Surveyor MS Pump consisted of a quaternary, low-pressure mixing pump with built-in solvent degassing and pulse dampening systems, for gradients from 25 to 2000 $\mu\text{L}/\text{min}$. The pump was able to hold up to four different solvents, which in this case were water, acetonitrile (ACN) and methanol (MeOH), all prepared with a 0.1% concentration of acetic acid to improve the chromatographic peak shape and provide a source of protons in reverse phase LC/MS⁴. The Surveyor PDA detector is a full-featured photo diode array (PDA) detector capable of scanning the ultraviolet-visible wavelength range from 190 to 800 nm. The dual-light source included a deuterium lamp for detection in the ultraviolet wavelength range (190 to 360 nm) and a tungsten-halogen lamp for detection in the visible wavelength range (360 to 800 nm).

A Thermo Electron LCQ MS detector was in series with the previously described equipment. An acquisition program was designed with the following parameters: a mass over charge ratio (m/z) range from 50 to 400.00 was chosen, covering the spectrum of the small molecules, possible degradation products and adducts, the ionization technique was positive ionization, the PDA was set with three UV channels (190, 280, 354 nm), and the flow was set at 150 $\mu\text{L}/\text{min}$. A solvent gradient of ACN:H₂O was used starting with a phase rich in an organic solvent, getting richer in the organic solvent up to a total of 10% of CAN and back to 90% of water for re-equilibration. The gradient lasted a total of 30 minutes, as seen in Figure 3-5. The injection volume was 3.0 μL .

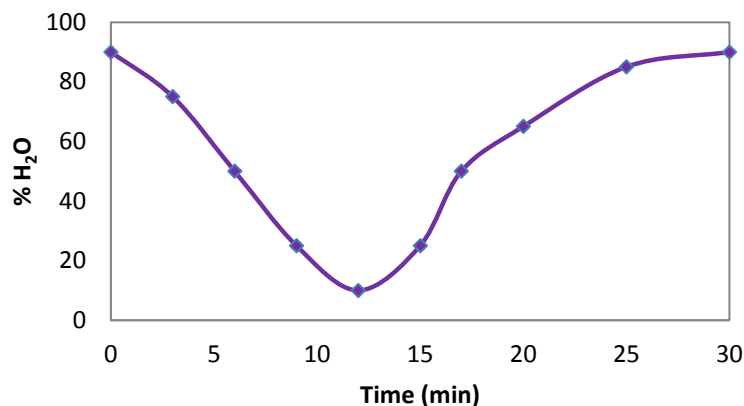


Figure 3-5. Gradient profile used in the LC-MS acquisition program.

A C18-Bidentate-Cogent column from MicroSolv Technology Corporation was used for the separation, with a height of 10 cm and an internal diameter of 2.1 mm. Both at the beginning and end of day, the column was re-equilibrated by flowing a gradient of 60:40 ACN:H₂O for approximately 30 minutes. Before each acquisition was taken, the column was washed with 10:90 ACN:H₂O for 10 minutes with an injection of 20 μ L of MeOH.

Once the Total Ion Chromatograph (TIC) was obtained for each time point, presence of the parent small molecule and degradation by-products was analyzed by utilizing a software tool called extracted chromatograph. An extracted chromatograph generates a chromatograph of a selected mass range and allows a better identification of specific m/z without background interference. The exact masses of the degradation products of each sample by the different degradation mechanisms are shown in Table 3-4.

Table 3-4. Exact masses of the degradation by-products of the samples.

Sample	Ion	Substitution		Dealkylation		Hofmann	
		R-OH	TMA	R-N-(CH ₃) ₂	CH ₃ OH	R-C=C	TMA
BTMA	150.13	108.06	59.07	135.1	32.03	N/A	

3QA1	178.16	136.09	59.07	163.14	32.03	118.08	59.07
4QA1	192.17	150.1	59.07	177.15	32.03	132.09	59.07
6QA1	220.21	178.14	59.07	205.18	32.03	160.13	59.07
3QA6	248.24	136.09	59.07	163.14	32.03	118.08 / 163.14	129.15 / 98.11

¹H Nuclear Magnetic Resonance Spectroscopy

A Bruker AV-360 NMR was used for the measurements. The sample was locked using D₂O as the solvent and the spectra were recorded at room temperature. The number of scans was set at 16. Proton chemical shifts were expressed in parts per million (ppm). The NMR data was analyzed using MestReNova software. A baseline correction was performed for every spectrum. The acquisitions were plotted in a stack to determine ppm ranges to perform the integrations. The integration ranges were saved and integrations were calculated as a batch process for all the spectra. Integrations were calibrated by setting the 1,4-dioxane value (approximately 3.8 ppm) as 1. Once the integrations were recorded for every range in each time point, they were divided by the correspondent amount of protons in the range. Subsequently, integrations were expressed as percentage of remaining quaternary ammonium group. This group mentioned before was used to compare stability of the different samples, i.e., the degradation profile of the QA group was plotted against time for each sample.

Summary

In this chapter, the synthetic routes for the samples used throughout this work were described. The degradation experiment was explained and the analytical techniques used to analyze the results were introduced.

-
1. Nuñez, S. A., & Hickner, M. A. (2012). Quantitative ¹H NMR analysis of chemical stabilities in anion-exchange membranes. *Acs Macro Letters*, 2(1), 49-52.
 2. Marino, M. G., & Kreuer, K. D. Alkaline Stability of Quaternary Ammonium Cations for Alkaline Fuel Cell Membranes and Ionic Liquids. *ChemSusChem* **2014**.
 3. Nuñez, S. A., & Hickner, M. A. (2012). Quantitative ¹H NMR analysis of chemical stabilities in anion-exchange membranes. *Acs Macro Letters*, 2(1), 49-52.
 4. Emmert, J., & No, C. (2006). Mobile Phase Additives for LC-MS, Part 1: Acids—The Most Common Choice.

Chapter 4

The influence of alkyl spacers and pendant chains on the stability of small molecules analogues for Anion Exchange Membranes by ^1H NMR

Introduction

As it was explained in Chapter 1, one of the most promising approaches for achieving enhanced stability in AEMs is by the incorporation of either alkyl spacers or pendant chains to increase the steric hindrance around the cation¹. This strategy was first explored by Tomoi² in resins with different lengths of alkyl spacers between the aromatic ring and the cation. After degradation in deionized water at 100-140 °C for 30 to 90 days, the resins with six carbon spacers showed extraordinary stability measured as strong base capacity titration.

Similarly, this work studies different small molecule analogues with various lengths of alkyl spacers (3, 4 and 6) and a pendant chain, to understand the extent of their influence in stability (Figure 4-1). The samples were subjected to a degradation test at 120°C in deuterated water in the presence of base (20 equivalents) and aliquots were taken at 0, 1, 2, 3, 6, 9, 12, 24 and 48 hours. These aliquots were measured by ^1H NMR with the specifications described in Chapter 3.

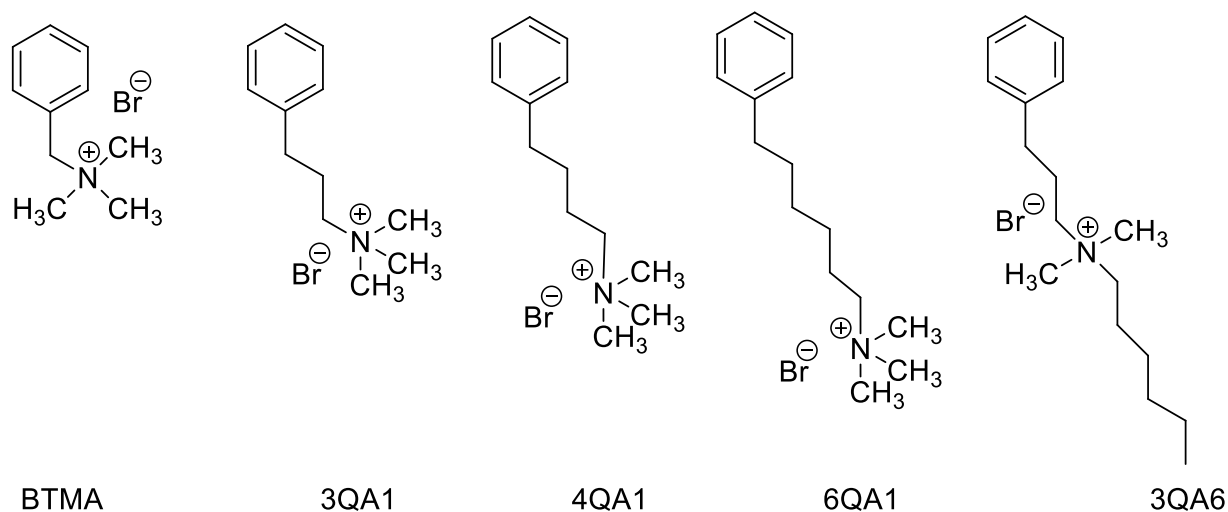


Figure 4-1. Small molecules with various lengths of alkyl spacers and pendant chains used for this work.

Stability

The small molecules synthesized are shown in Figure 4-1. BTMA is the commonly used *benzyltrimethylammonium* and the other samples were designed to have increasing numbers of carbon alkyl spacers. Last, a small molecule with a three-carbon alkyl spacer and a six-carbon pendant chain was synthesized. The NMR spectrums obtained from the NMR Facility at Penn State were analyzed using MestReNova software. The spectrums for each of the samples are in the Appendix.

The spectra at the different time points were compared to the spectrum at time zero. An example of the time-stacked spectra of BTMA is shown in Figure 4-2. The atoms chosen to describe the stability were the hydrogens of the methyl attached to the nitrogen (TMA). These protons at time zero represent 100% of abundance; the subsequent time points were then compared. The degradation profile of the samples after the degradation treatment is shown in Figure 4-2.

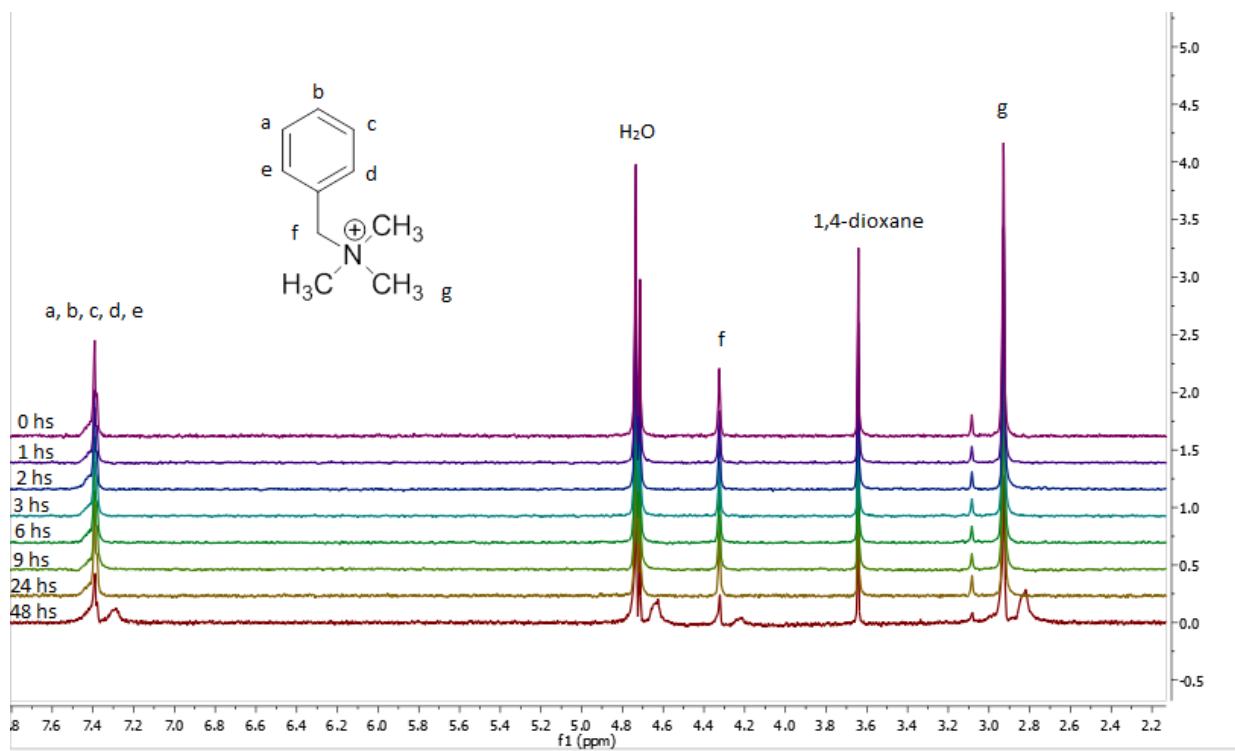


Figure 4-2. Comparison of spectrums from time 0 to time 48 hours on BTMA sample.

A more detailed inspection of the spectrum at chemical shifts between 2.9 and 2.95 ppm correspondent to the trimethylammonium moiety is shown below in Figure 4-3. Degradation was measured as the relative change in the TMA peak of the spectrum. The relative degradation was plotted for every sample at each time point as shown in Figure 4-5.

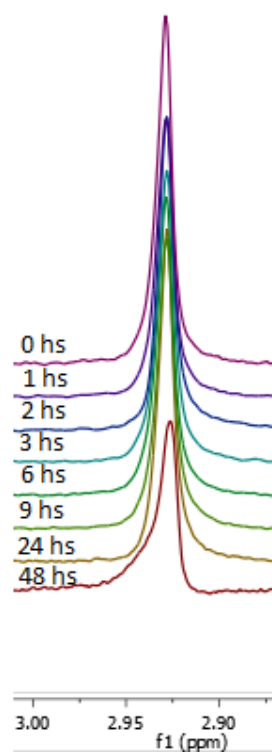


Figure 4-3. TMA degradation profile in BTMA sample.

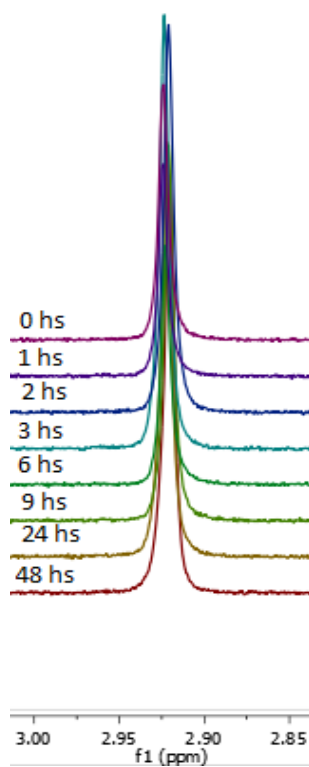


Figure 4-4. TMA degradation profile in 6QA1 sample.

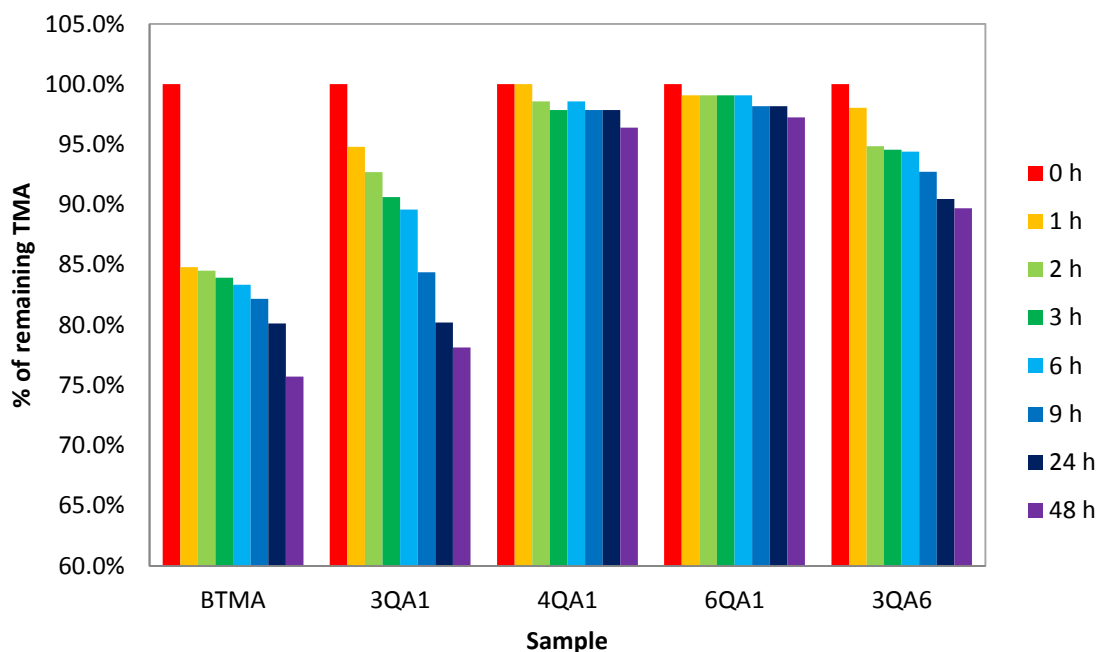


Figure 4-5. Degradation profile of BTMA, 3QA1, 4QA1, 6QA1 and 3QA6 in the presence of NaOH (20 equivalents) at 120°C over 48 hours.

As expected, BTMA has the highest degradation in the course of the study, with a total of 75.7% of remaining TMA. Figure 4-3 shows the progression of the degradation for the TMA moiety for the BTMA sample. 3QA1 showed 2.4% less degradation than BTMA with a total of 78.1% of remaining TMA. 4QA1 and 6QA1 showed even better stabilities with 96.4 and 97% respectively, being this last one the most stable small molecule in the sample pool. Figure 4-4 shows the degradation profile of the TMA in sample 6QA1. Degradation profiles of the other samples are shown in the Appendix. This data supports the idea that as the length of the alkyl spacer increases, the total degradation decreases, confirming the initial hypothesis that alkyl spacers are a feasible strategy for enhanced stability. This proves that steric hindrance serves as a mean of decreasing the rate of hydroxide attack to the cations.

As previously explained, sample 3QA6 was designed to understand the influence of pendant chains in the stability of small molecule cations. The degradation profile of 3QA6 reveals that this sample has better hydroxide stability than both BTMA and 3QA1 - this last one being the analogue small molecule without the pendant chain, as they both have a three-carbon alkyl chain between the benzene ring and the trimethylammonium, with a percentage of remaining TMA of 90%. This results help explain that the addition of pendant chains does not provide substantial enhanced stability for small molecule cations. The rates of degradation of the samples were determined by the plot of the natural logarithm of the concentration of the remaining TMA as a function of time using a pseudo-first-order approximation (Figure 4-6), given that the concentration of base (20 equivalents) is in excess and can be assumed constant during the course of the study³.

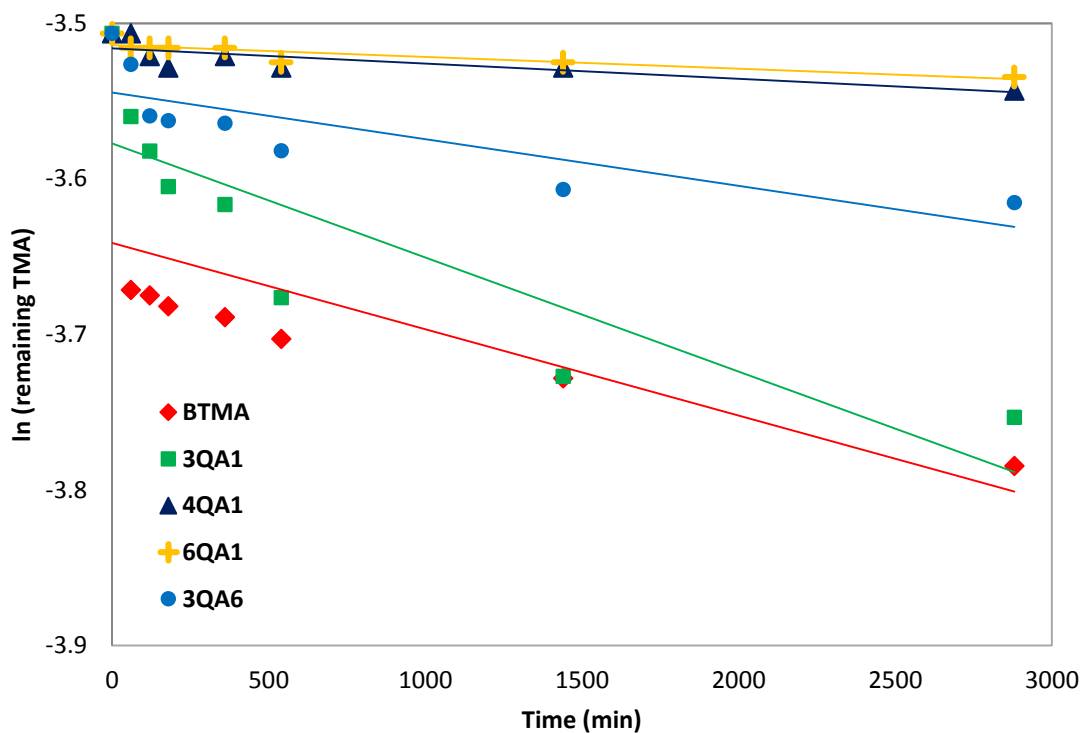


Figure 4-6. Plot of the rate of degradation of samples BTMA (♦), 3QA1 (■), 4QA1 (▲), 6QA1 (+) and 3QA6 (●).

As it can be seen in the plot, the fitting for samples BTMA and 3QA1 have some error translated from the great amount of degradation in the first hour, as it can be seen in Figure 4-5. Table 4-1 summarizes the kinetic rates of degradation. 6QA1 shows the best stability compared to the other samples with a half-life of 1444.1 hours, an order of magnitude greater than BTMA.

Table 4-1. Degradation constants and half-lives of samples BTMA, 3QA1, 4QA1, 6QA1 and 3QA6.

	k ($M^{-1} \text{min}^{-1}$) 10^{-5}	$t_{1/2}$
BTMA	6	192.5
3QA1	7	165.0
4QA1	1	1155.2
6QA1	0.8	1444.1
3QA6	3	385.1

Interestingly enough, the half-life of 3QA1 was smaller than that of BTMA, with 165 hours for the first one and 192.5 for the second one, although the ^1H NMR degradation profile (Figure 4-2) showed a final concentration of BTMA of 75.7%, while the final concentration of 3QA1 was of 78.1%. This difference can also be explained by the error in the fitting derived from the big drop in stability in the first hour of the degradation experiment.

Additionally, it is interesting to compare the rates of 3QA1 and 3QA6, since the former has not only the three carbon alkyl spacer of 3QA1, but also a pendant chain of six carbons. As it can be seen from the data, the half-life of 3QA6 is over the double of that of 3QA1, with 385.1 hours for the first and 192.5 for the second, meaning that pendant chains contribute to enhanced stability as they add steric shielding around the cation. However, arising from the extraordinary half-life of 1444.1 hours of 6QA1, it seems that alkyl spacers provide a greater effect on stability than the summation of both strategies.

Conclusions

^1H NMR was used to determine the degradation rate of samples with different lengths of alkyl spacers and pendant chains. The degradation profile showed that as the length of the alkyl spacers increases, the degradation rate decreases, as seen in samples 3QA1, 4QA1 and 6QA1. When comparing samples 3QA1 and 3QA6, it became evident that the pendant chain contributes to the steric shielding and helps decrease degradation. However, sample 6QA1 without any pendant chain and with three more carbons than 3QA1, showed exceptional stability with only 10% degradation after 48 hours in the presence of base.

As a corollary, it would be interesting to investigate the stability of a small molecule cation like 6QA1 with the addition of a pendant chain. It would be expected to present higher stability than 6QA1, as it happened between 3QA1 and 3QA6 in this work.

-
1. Kreuer, K. D. (2013). Ion conducting membranes for fuel cells and other electrochemical devices. *Chemistry of Materials*, 26(1), 361-380.
 2. Tomoi, M.; Yamaguchi, K.; Ando, R.; Kantake, Y.; Aosaki, Y.; Kubota, H. Synthesis and Thermal Stability of Novel Anion Exchange Resins with Spacer Chains. *Journal of Applied Polymer Science* 1997, 64, 1161–1167.
 3. Nuñez, S. A.; Hickner, M. A. Quantitative ¹H NMR Analysis of Chemical Stabilities in Anion-Exchange Membranes. *ACS Macro Lett.* 2013, 2, 49–52.

Chapter 5

Identification of degradation mechanisms by LC-MS

Introduction

In Chapter 2, the different degradation mechanisms that AEMs can undergo were explained. It became evident that the chemistry of the cations has a big influence on the degradation pathways that can occur. For example, cations without the presence of β -hydrogens do not suffer from the Hofmann elimination mechanism. In Chapter 4 it was demonstrated that alkyl spacers are a feasible strategy for achieving enhanced stability in small molecule cations. It is also the aim of this work to understand and identify the degradation mechanisms. One way to do this is by identifying the degradation by-products, since they are distinct and characteristic for each degradation mechanism in each sample. The technique chosen was liquid chromatography – mass spectrometry (LC-MS), a separation and characterization technique, respectively, further explained in Chapter 2.

Identification of degradation by-products and mechanisms

Aliquots of the degraded samples at the different time points were analyzed by LC-MS with a batch program described in Chapter 3. The degradation mechanisms for each sample are shown in the Appendix A.

The outcome in the LCMS analysis is a chromatograph of the abundance as a function of elution time. This chromatograph is called total ion chromatograph (TIC). However, if the concentration of some components of the sample is too small, a component may not be observed

as a clear peak in the TIC. An extracted ion chromatograph (EIC) can be generated from a TIC, and it can show the chromatograph of a specific mass or mass range. For this reason, an EIC was generated for each time point in the mass ranges that correspond to the degradation by-products, described in Table 3-4, plus minus one unit.

An example of the TIC of 4QA1 is shown below in Figure 5-1. The non-degraded sample of m/z 192.17 elutes between 9.43 and 10.03 minutes at both time 0 (top) and time 24 hours (bottom) respectively. The ion can be seen as an isolated peak because of its concentration. The peak seen at time 21.81 minutes is some background contamination and was observed in all the chromatographs taken. The spectrum at retention time 10.10 minutes is shown in Figure 5-2, where the intensity and m/z of said peak can be observed. The spectrums were used to identify the by-products.

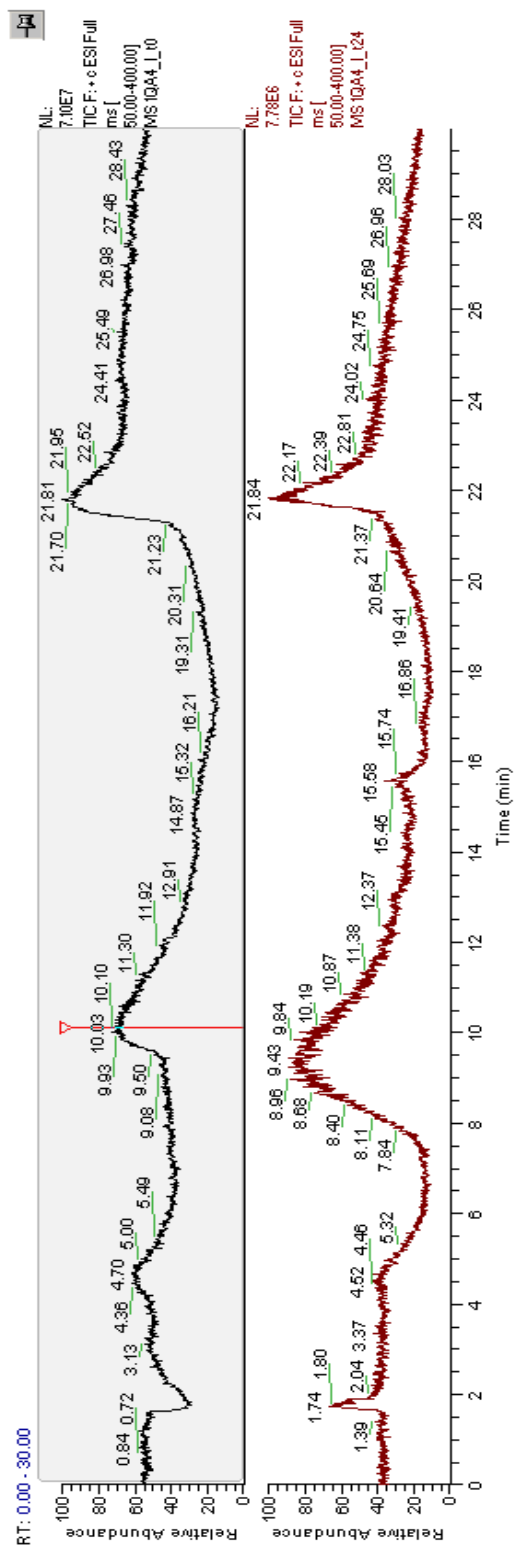


Figure 5-1. TIC of sample 4QA1 at time 0 (top) and time 24 h (bottom).

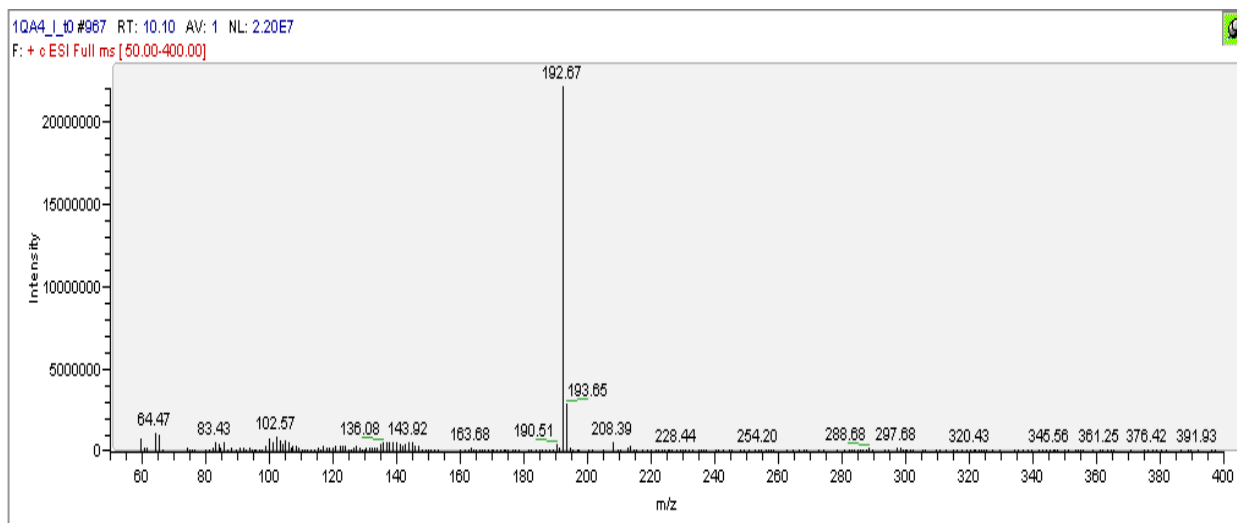


Figure 5-2. Spectrum of sample 4QA1 at time 0, at retention time 10.10 minutes.

The chromatographs at each time point were analyzed for the samples. However, it was observed that the most information could be obtained from the last time points, where the degradation by-products were most concentrated. The TIC of BTMA after 24 hours of degradation is shown in Figure 5-3. An EIC was generated for the non-degraded ion and the two degradation by-products (methanol and trimethylamine were not analyzed because of the less sensitivity of the equipment at low m/z numbers).

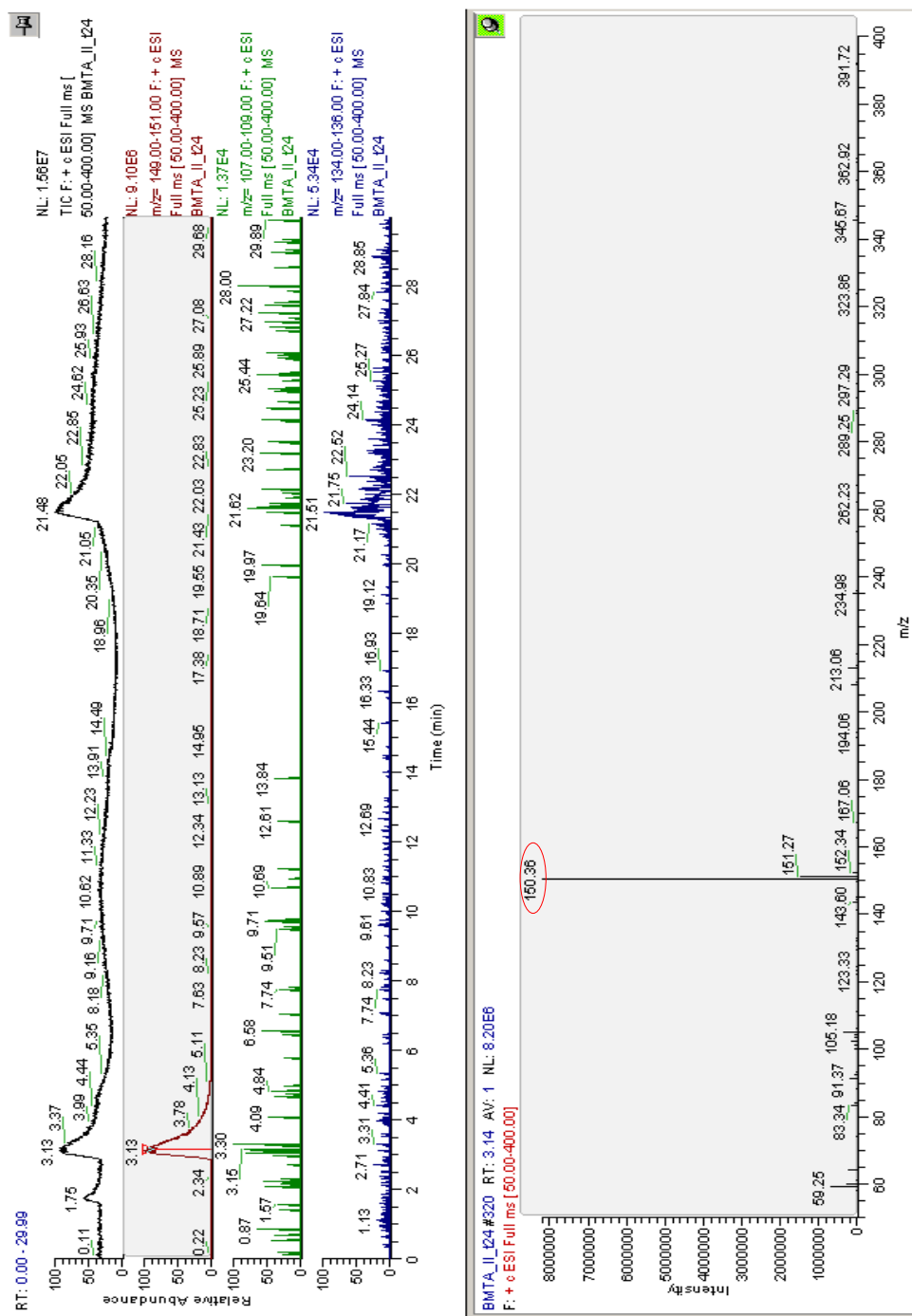


Figure 5-3. TIC (top), EICs for the non-degraded compound and the two degradation by-products and spectrum at retention time 3.14 minutes (bottom) for sample BTMA.

For BTMA, the degradation by-product of substitution was not observed as it can be seen in Figure 5-4 (m/z 108), whereas the degradation by-product of dealkylation was observed (m/z 135).

For sample 3QA1, the same analysis was done as shown in Figure 5-4.

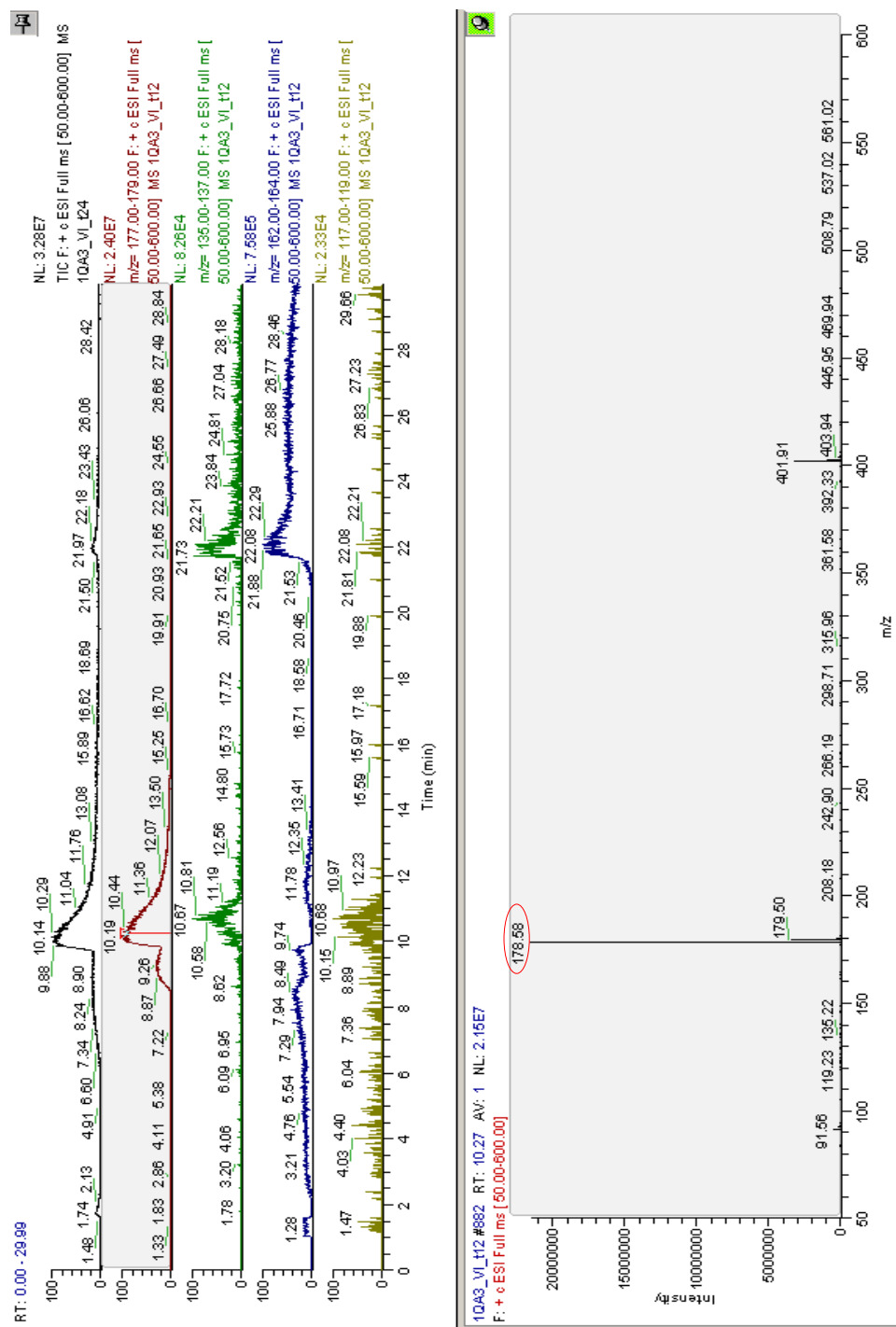


Figure 5-4. TIC (top), EICs for the non-degraded compound and the two degradation by-products and spectrum at retention time 10.27 minutes (bottom) for sample 3QA1.

The non-degraded compound is seen in the first EIC, eluting at 10.19 minutes. The product of substitution is observed at both 10 and 21 minutes. In the spectrum at the bottom of the picture, both this m/z numbers can be observed. The product of dealkylation (m/z 163) can be seen throughout the whole elution range and can thus be considered as part of the background and not as a specific by-product. The presence of this m/z number was checked at time 0 and the EIC generated was similar to the one for time 24 hours. The product of Hofmann elimination could not be distinguished either.

Similarly, sample 4QA1 was analyzed. Figure 5-5 shows the EIC for the non-degraded compound and the three suspected degradation by-products. The compound elutes at approximately 9.43 minutes. The product of substitution, 4-phenyl-1-butanol, is observed at approximately 3.4 minutes. The spectrum at the bottom shows the m/z of 150 for identifying the substitution mechanism. There is no evidence of the dealkylation mechanisms taking place; however, 4-phenyl-1-butene elutes at approximately 21.7 minutes. The order in which the compounds elute is not random and helps confirm the presence of each of the eluents. The solvent gradient starts with high concentration of aqueous phase, which promotes the elution of the most polar components of the mixture, in this case, the alcohol. The ammonium elutes later than the alcohol, as it has less polarity. Additionally, the C18 column is highly hydrophobic and it binds with the most hydrophobic components. The last compound to elute is the alkene, as it is the less polar of all and stays longer in the porous silicate.

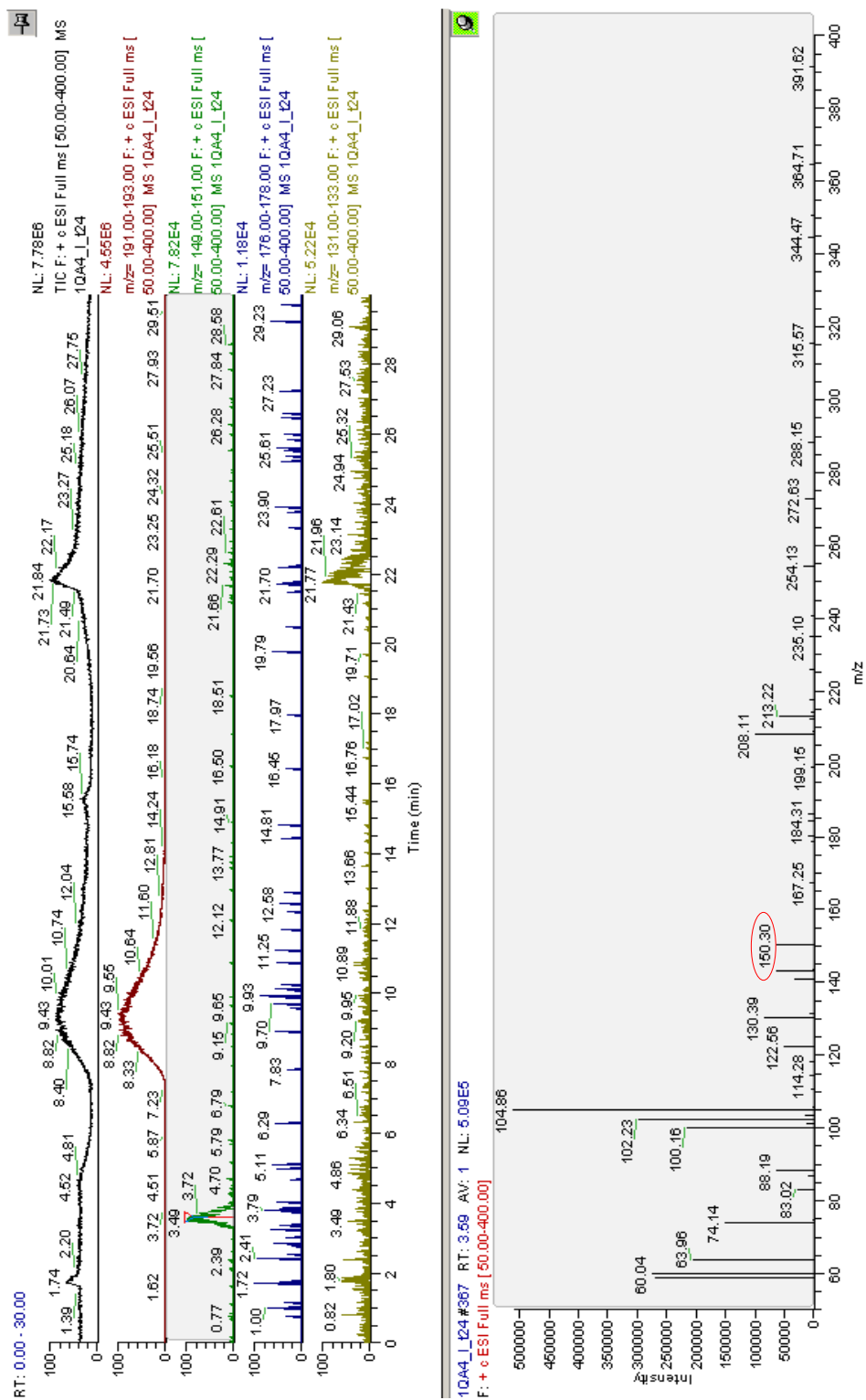


Figure 5-5. TIC and EICs for sample 4QA1 at time point 24 hours.

Sample 6QA1 was analyzed in a similar fashion as sample 4QA1. A TIC and EICs for the three degradation by-products at time point 24 hours is shown in Figure 5-6. The spectrum at the bottom shows the m/z of 178, for the substitution by-product. Even though they are not in the same intensity, the degradation by-products of all three mechanisms can be identified by the extraction as seen in the figure.

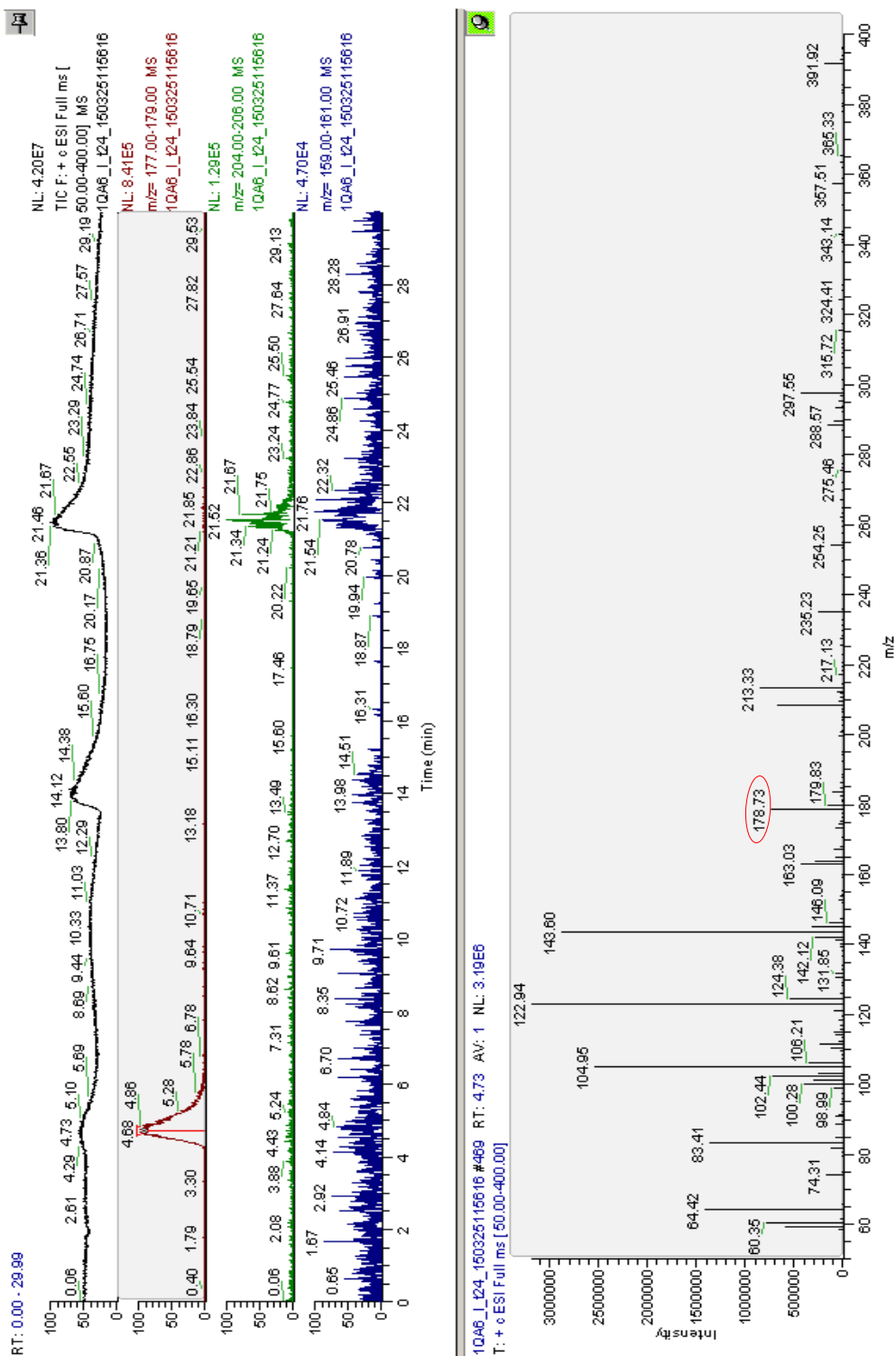


Figure 5-6. TIC and EICs for sample 6QA1 at time point 24 hours.

Sample 3QA6 also showed interesting results, seen in Figure 5-7. The total degradation of sample 3QA6 corresponds to 59.6%. The degradation by-products identified in the 48 hour sample were the products of substitution (m/z 136) and dealkylation (m/z 163), with a total of 0.64% for the first one and 8.4% for the second one. The spectrum of the degradation by-product of dealkylation is shown in Figure 5-7 (bottom). Two possible products of the Hofmann elimination were expected. However, none of them were observed in the extraction.

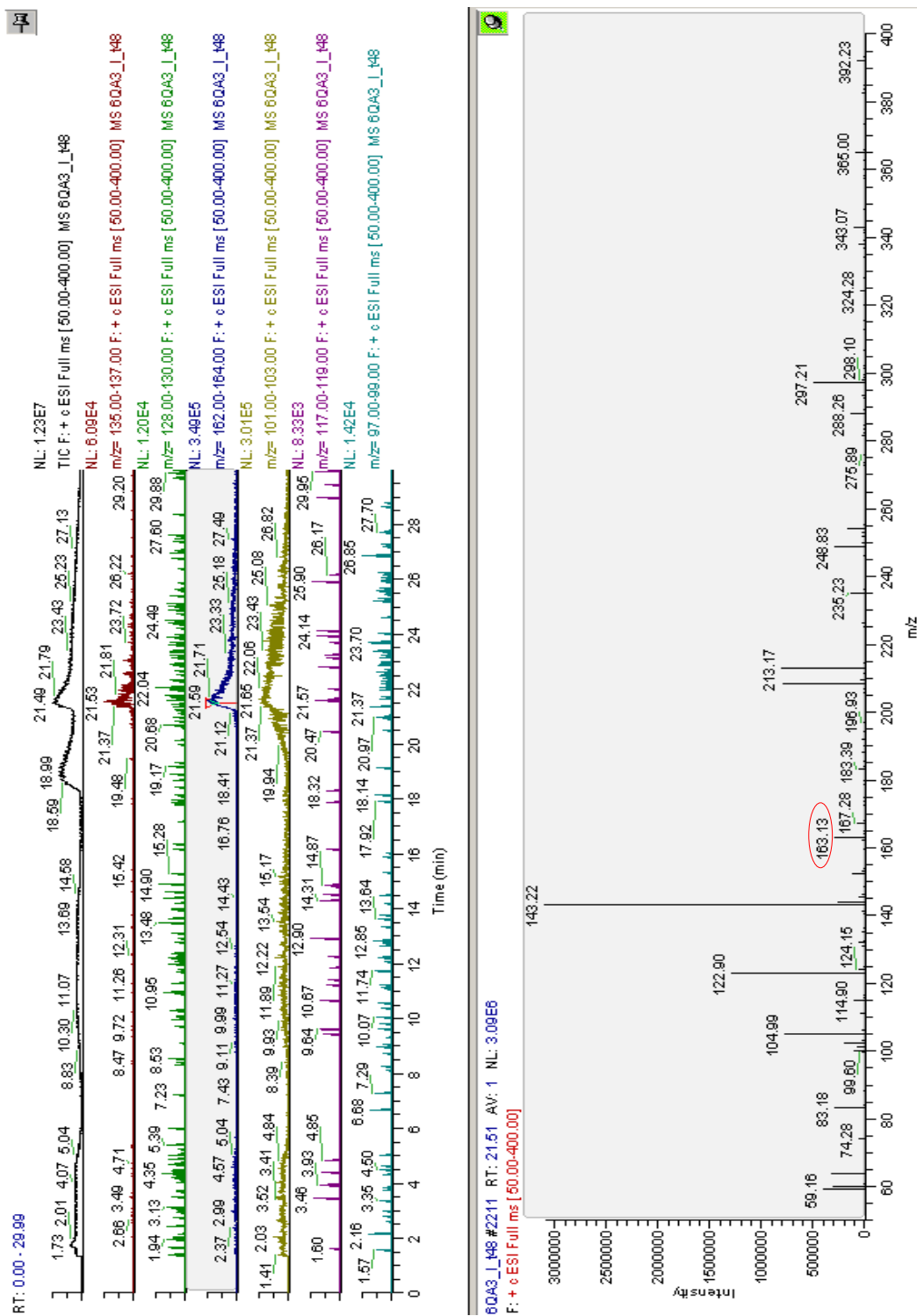


Figure 5-7. TIC and EICs for sample 3QA6 at time point 24 hours.

A summary of the degradation by-products of the three mechanisms studied is shown in Table 5-1. All of the samples show to undergo the substitution degradation mechanism. Dealkylation is presented in samples BTMA, 6QA1 and 3QA6, while Hofmann elimination can be seen in 4QA1 and 6QA1.

Table 5-1. Degradation by-products of samples by LCMS.

Sample	Substitution	Dealkylation	Elimination
BTMA	X	✓	N/A
3QA1	✓	X	X
4QA1	✓	X	✓
6QA1	✓	✓	✓
3QA6	✓	✓	X

Summary

This chapter has described a chromatographic and spectroscopic method for analyzing the degradation mechanisms of samples containing alkyl spacers and pendant chains. It has been demonstrated that one strategy for identifying the degradation mechanisms is to analyze the degradation by-products.

It is observed that the total degradation, considered as the sum of the individual degradations for each sample, does not coincide with the degradation obtained with ^1H NMR. LCMS is used as a qualitative technique to identify degradation mechanisms while ^1H NMR is a quantitative technique used to determine degradation rates. This depicts the importance of using both techniques to have an overall understanding of the stability and degradation of the samples.

Chapter 6

Analysis of degradation by-products of a PPO-based AEM

The previous chapters reported the degradation mechanisms and degradation rates of analogue small molecule analogues to AEMs to understand the extent of the influence of carbon alkyl spacers and pendant chains in the stability of the molecules. It was clearly demonstrated that both these strategies are useful for the design of more stable membranes.

In order to enlighten the aspects behind anion exchange membrane degradation, a PPO-based membrane with a hexyl pendant chain¹ (Figure 6-1) provided by Liang Zhu from the Hickner Group was degraded and the degradation by-products were studied by ¹H NMR. The membrane was first transformed into its hydroxide form by immersion in 1M NaOH for 24 hours.

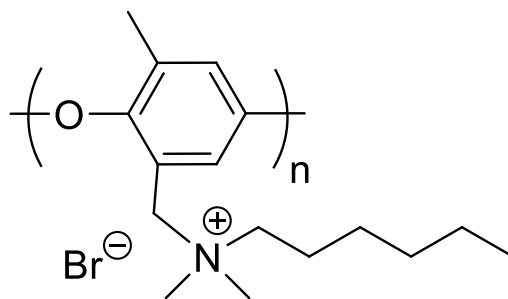


Figure 6-1. PPO-1QA6.

The degradation treatment was performed similarly to the small molecules; a square of membrane sample approximately 1.5 cm by 1.5 cm (50-70 microns thick) was cut and submerged in a solution of 1M NaOD in D₂O at 120°C. Aliquots were taken at intervals of 24 hours, measured by ¹H NMR and compared to the spectrum taken at time zero. Before the first 72 hours, there was no major change in the spectrum as seen in Figure 6-2.

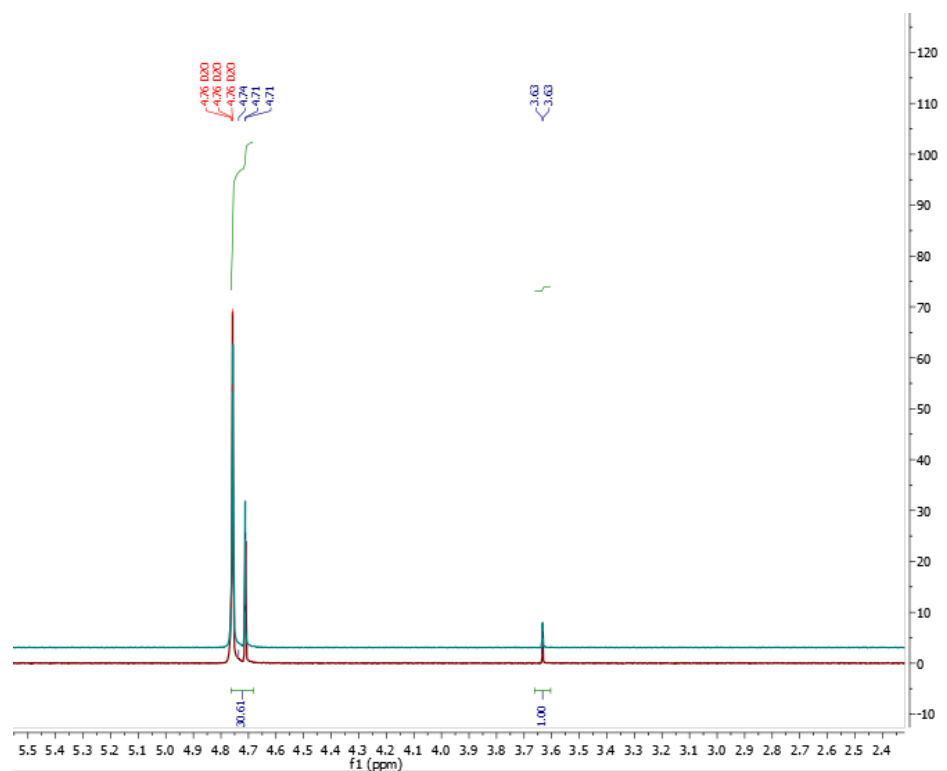


Figure 6-2. ^1H NMR spectrum at time zero (blue) and 72 hours (red).

Even though the membrane did not dissolve and appeared to remain structurally untouched, successive aliquots started to show peaks that can be considered to come from the degradation by-products. A very interesting spectrum was given by the aliquot at time 120 hours. This sample was measured by a 500 Hz Bruker NMR spectrum to be able to obtain more information from it. The spectrum is shown in Figure 6-3. A water suppression tool was used because of the intensity of the water-related peak. The peak at 3.6 ppm corresponds to the internal standard (1,4-dioxane). Additionally, a COSY NMR spectrum was taken to show possible connections between hydrogens in adjacent carbon atoms (Figure 6-4).

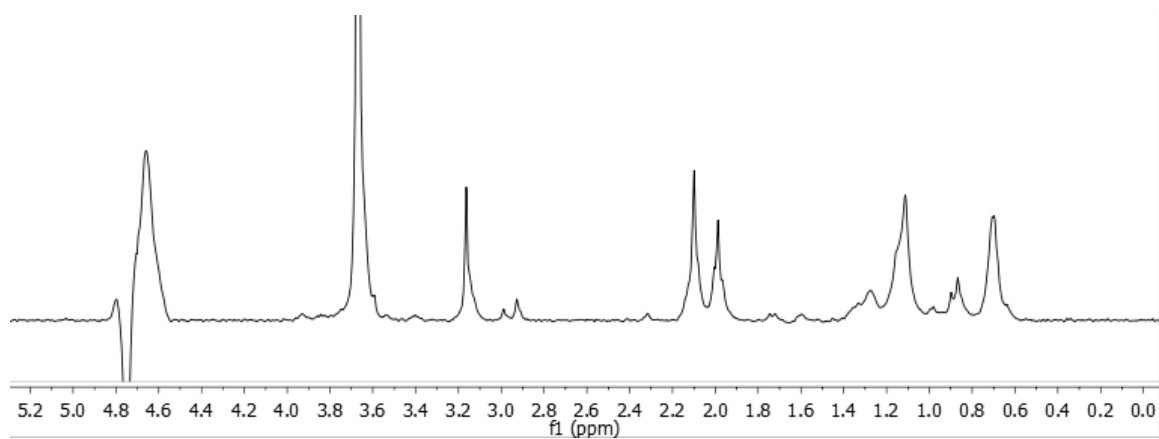


Figure 6-3. ^1H NMR spectrum at 120 hours.

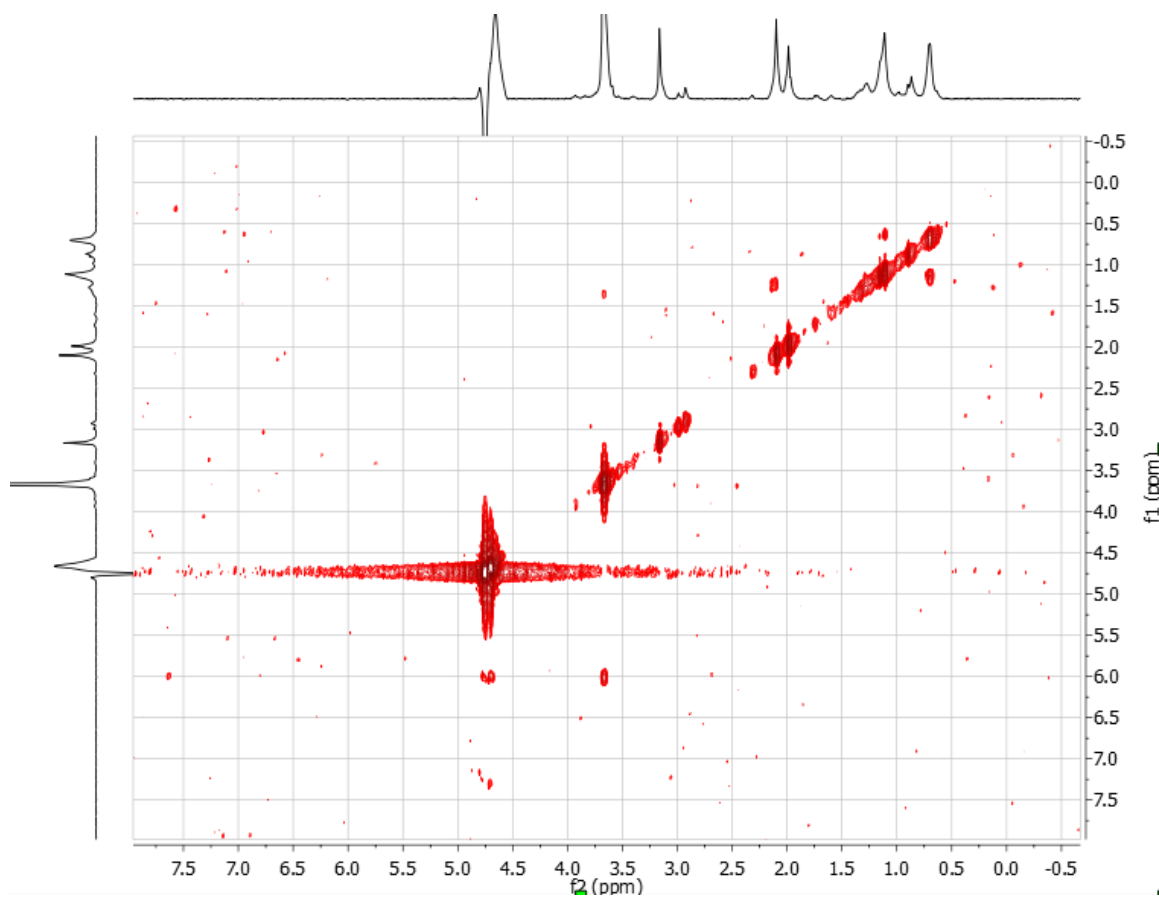


Figure 6-4. COSY NMR spectrum at 120 hours.

Although it was difficult to do a complete assignment of the new peaks to some or part of the suspected degradation by-products, some important conclusions can be drawn from this experiment:

1. The absence of aromatic signals (7-8 ppm, region not shown in the spectrum) shows the no formation of aromatic fragments, so it can be concluded that there is no significant backbone degradation.
2. The intense 1,4-dioxane peak at 3.6 ppm prevents clear identification of alcoholic fragments in the 3-4 ppm region.
3. The presence of a long aliphatic chain is sustained by the peaks at 0.4-1.5 ppm region, as well as the off-diagonal peaks in the same region in the COSY experiment (Figure 6-5), which suggest close connection between these two protons.

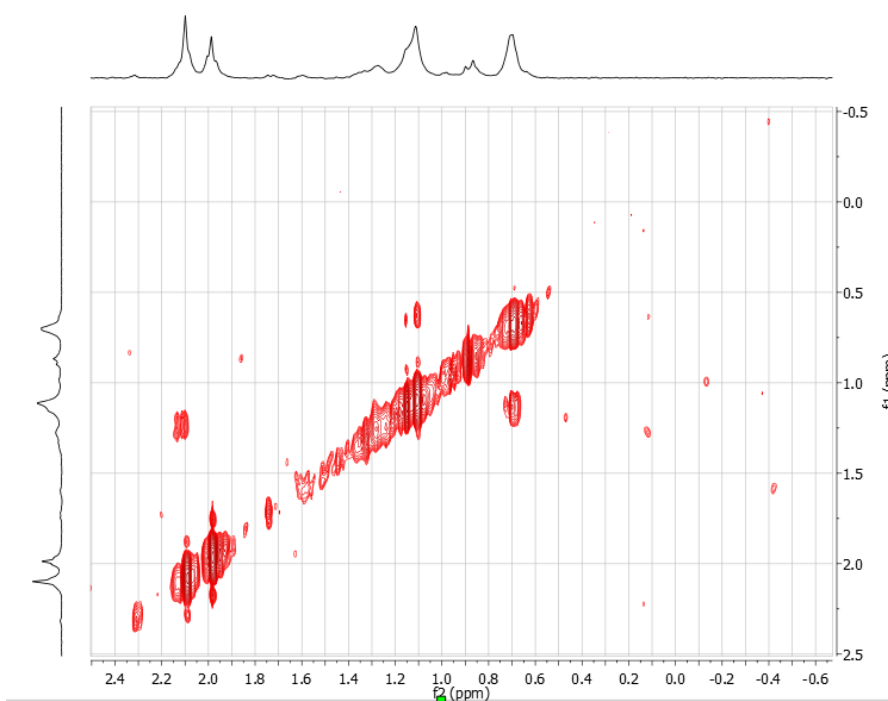


Figure 6-5. COSY NMR spectrum, closer look at region 0.4 – 1.5 ppm.

- The possibility of amine(s) formation can be stated by the two signals at 2 ppm and the one at 3.2 ppm.
- The absence of peaks at approximately 5 ppm suggests the lack of alkene compounds.

The information given before suggests that the substitution mechanism is the most likely to occur, shown in Figure 6-6.

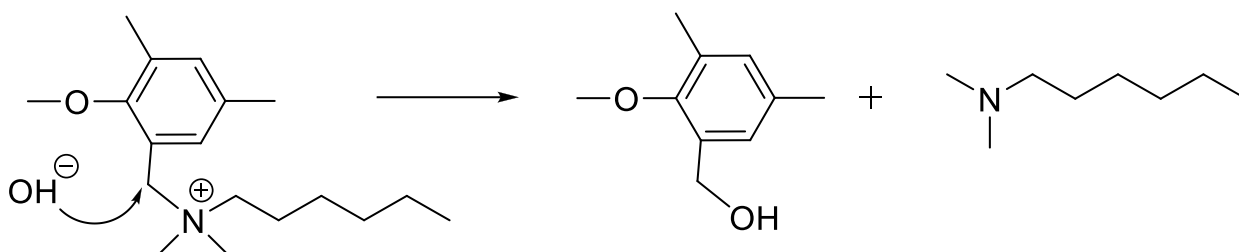


Figure 6-6. Substitution mechanism in PPO-1QA6.

In order to confirm the suspected degradation mechanism, FTIR measurements of the membrane could be performed to analyze the presence of the benzyl alcohol that would be remaining in the membrane.

More information can be taken from this type of experiments by increasing the degradation rate (increasing the temperature and/or the concentration of base), to increase the concentration of the products and increase the resolution of the NMR spectrums. Also, a TOCSY experiment can be performed to analyze further connections between spins.

1. Li, N., Leng, Y., Hickner, M. A., & Wang, C. Y. (2013). Highly stable, anion conductive, comb-shaped copolymers for alkaline fuel cells. *Journal of the American Chemical Society*, 135(27), 10124-10133.

Chapter 7

Conclusions and future work

Conclusions

The work performed in this thesis has supported the feasibility of using alkyl spacers and pendant chains as strategies for creating a steric hindrance around the quaternary ammonium in anion exchange membranes for enhanced stability. Small molecules containing different lengths of alkyl spacers were synthesized and subjected to a degradation experiment. Its relative stability was measured by ^1H NMR, which showed that the degradation rate decreased with increasing spacer chain length. A sample containing a spacer chain and a pendant chain was also analyzed, showing that compared to its analogue with only the spacer chain, stability was increased; however, when compared to a small molecule with a longer alkyl spacer only, its stability was not as high as for the second one. This data provided the information that alkyl spacers would be the preferred method for cation stability enhancement.

LC-MS was used to qualitatively identify the degradation mechanisms. It was previously believed that there was one preferred degradation mechanism for anion exchange membranes. However, the results in this work show that various mechanisms occur simultaneously and that they depend strongly on the chemistry of the molecule or membrane. The sample with the longest alkyl spacer presented the three of the mechanisms studied, while most of the other samples presented only two of them. Except from BTMA, the samples with the fastest degradation rates (3QA1, 4QA1, 3QA6) were degraded by a substitution-type mechanism, while the most stable sample (1QA6) presented all three types of the major degradation mechanisms. It is possible that the substitution degradation mechanism is the fastest of all the possible ones, making the

compounds that degraded by this mechanism, do it at a faster rate than the ones that have competing mechanisms.

Additionally, FTIR measurements of the degraded PPO-based membrane would help confirm the suspected degradation mechanism.

Future work

This work has clearly determined the use of alkyl spacers as a method for enhanced small molecule stability. A step forward in designing more stable membranes would be to translate this strategy to anion exchange membranes and study their stability. Additionally, testing membranes with alkyl spacers in fuel cells would give a better idea of their performance in a real fuel cell environment. Other properties such as mechanical strength, ion exchange capacity and conductivity should be studied in order to confirm that alkyl spacers are the path into more stable membranes.

More detailed information on the degradation mechanisms could be obtained if the degradation rate of the small molecules is increased, by increasing the hydroxide concentration and/or the temperature of the experiment. Another way of doing this could be by increasing the intervals between aliquots to elongate the total degradation time of the small molecules. Additionally, if the background contamination is lowered, the peaks of the degradation by-products might be seen in the total ion chromatograph without the need of using the extracted ion chromatograph tool. Another possibility of confirming the degradation by-products present on the mixture could be to synthesize the suspected degradation by-products and analyzing their

behavior in the LC-MS, as well as using other tools for their identification, such as the UV-Vis portion of the LC-MS.

Appendix A

^1H NMR spectra and degradation mechanisms for each sample

NMR spectra for each sample. The peak at approximately 4.8 ppm corresponds to water.

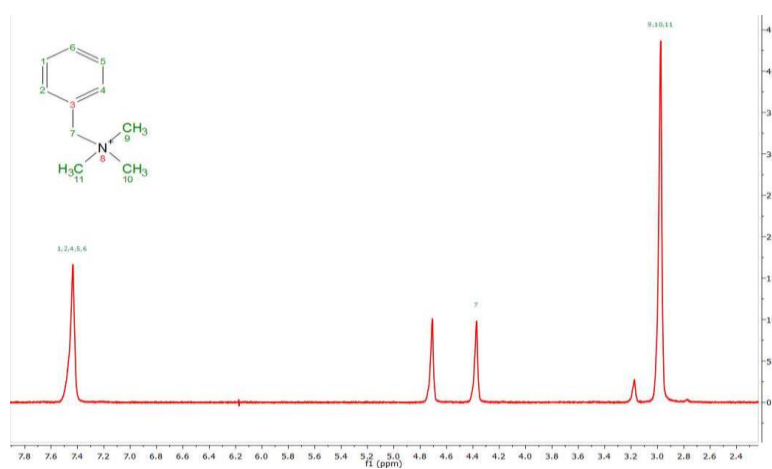


Figure A-1. NMR spectrum for sample BTMA. The peak at 3.17 ppm is suspected to be an impurity.

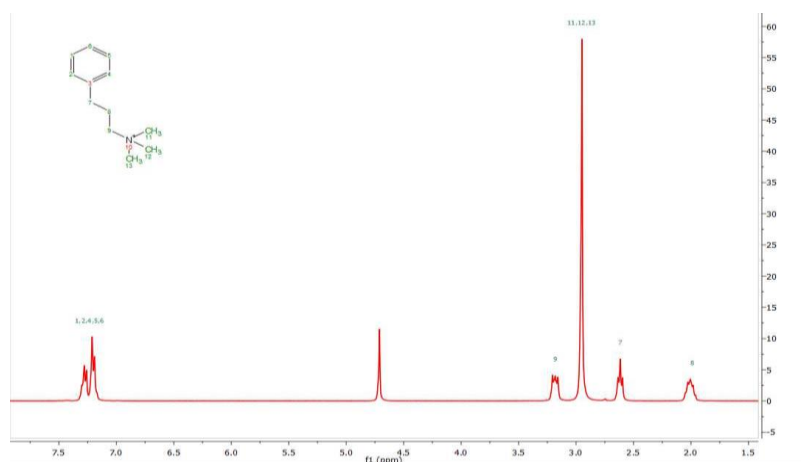


Figure A-2. NMR spectrum for sample 3QA1.

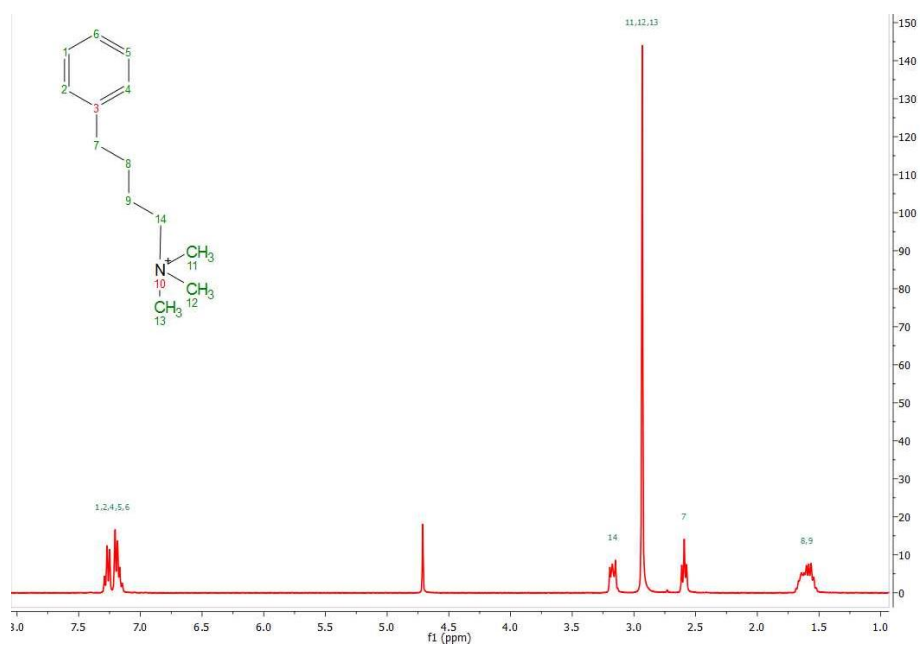


Figure A-3. NMR spectrum for sample 4QA1.

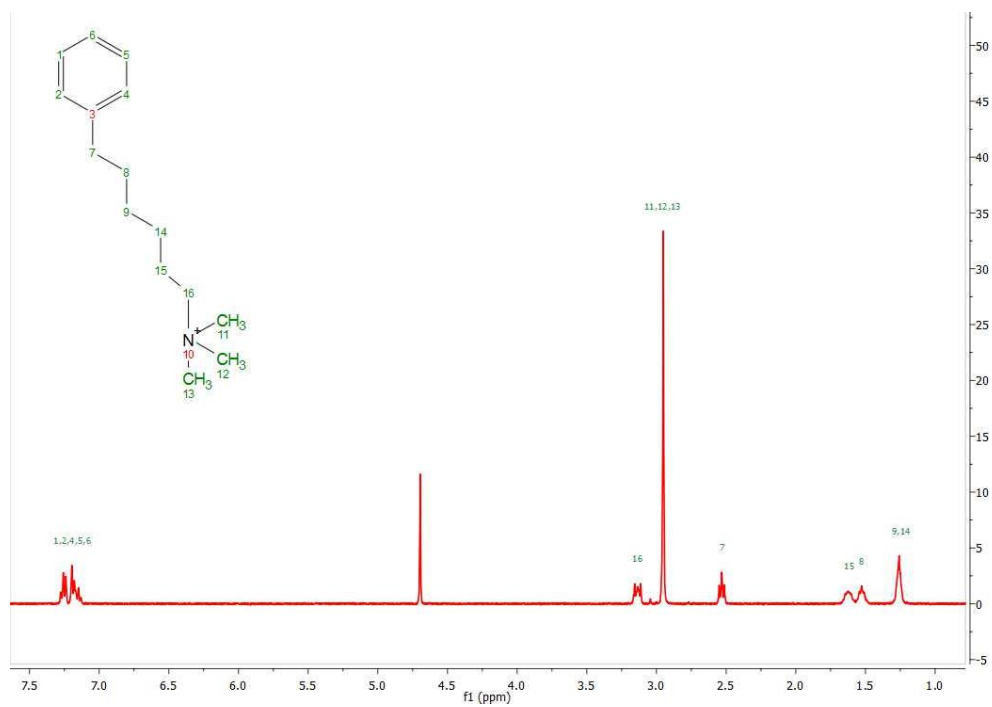


Figure A-4. NMR for sample 6QA1.

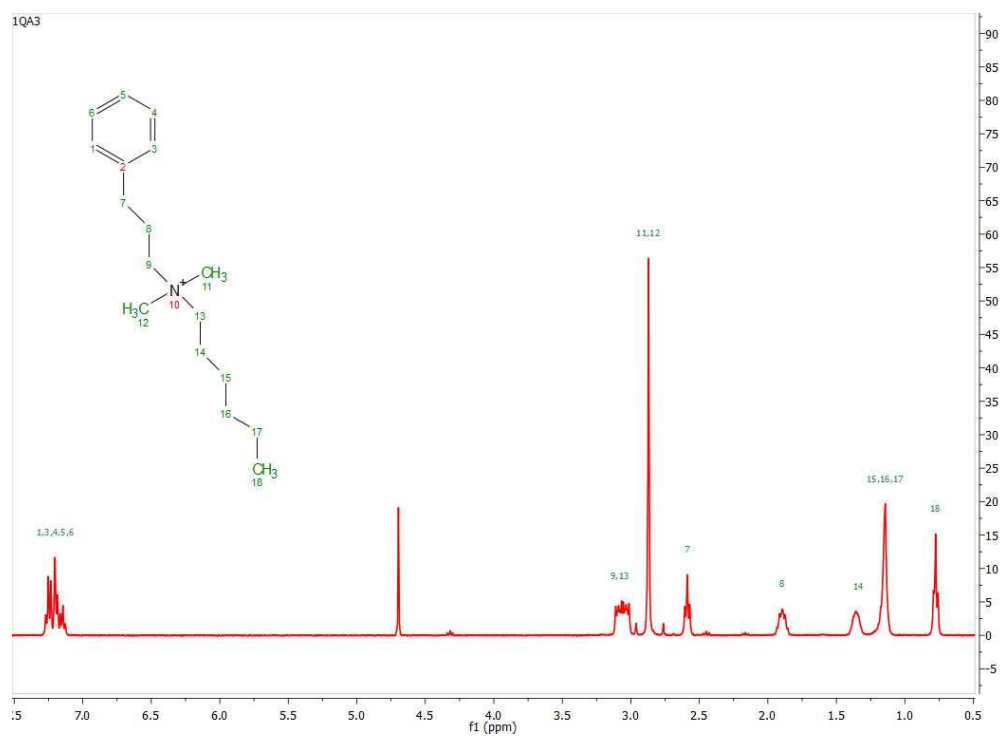


Figure A-5. NMR for 3QA6.

Degradation mechanisms for each sample:

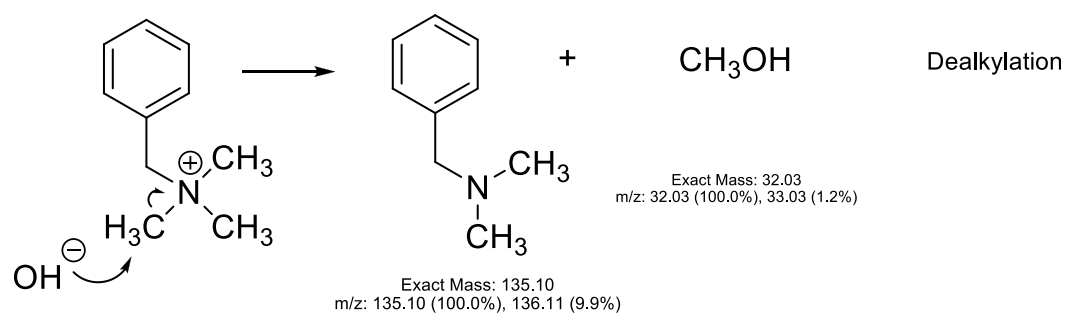
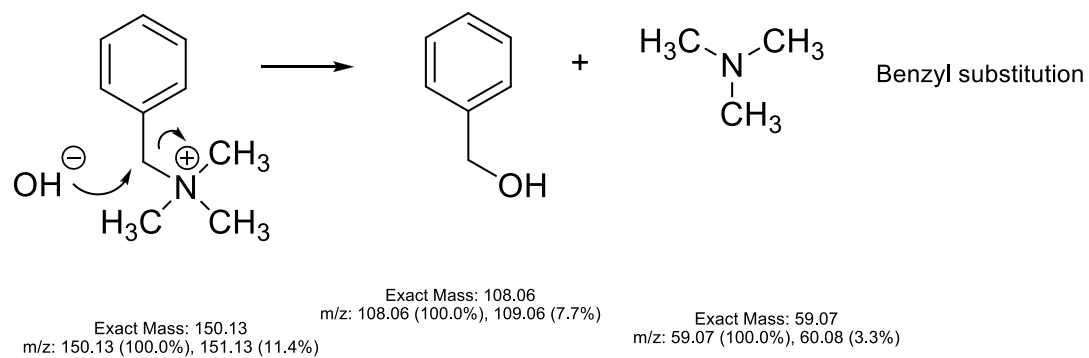


Figure A-6. Degradation mechanisms for sample BTMA.

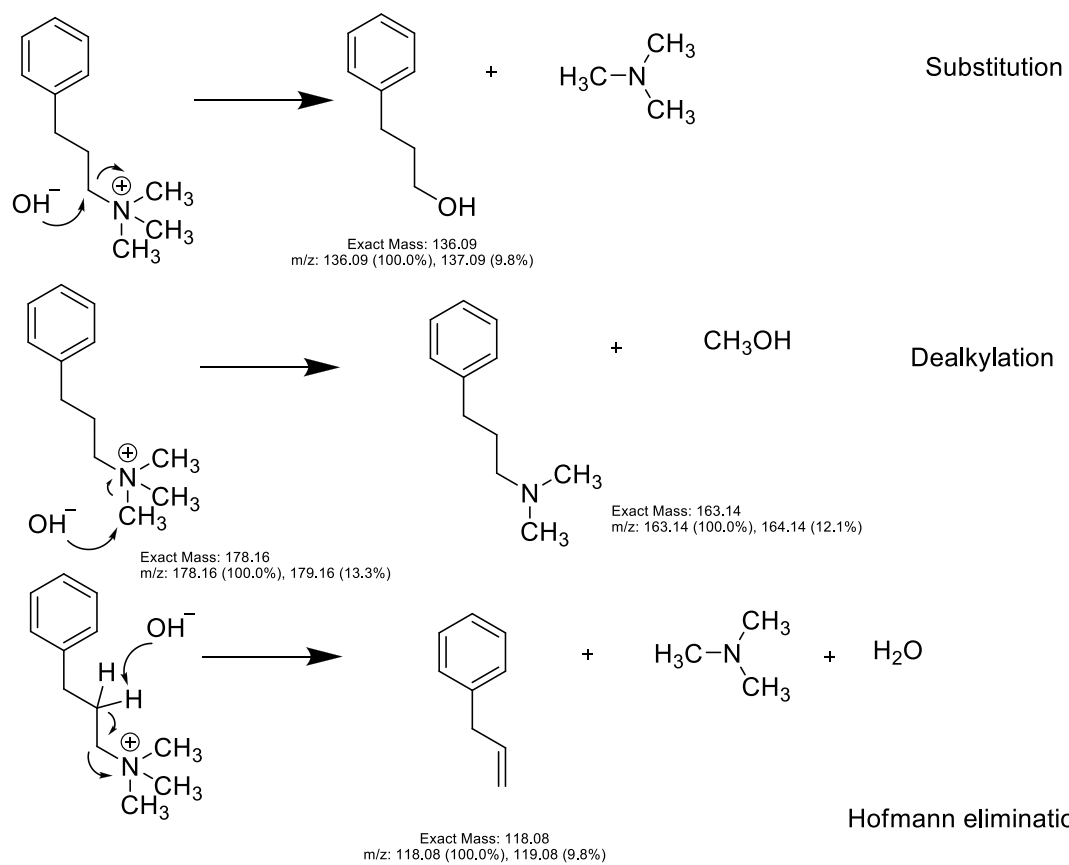


Figure A-7. Degradation mechanisms for sample 3QA1.

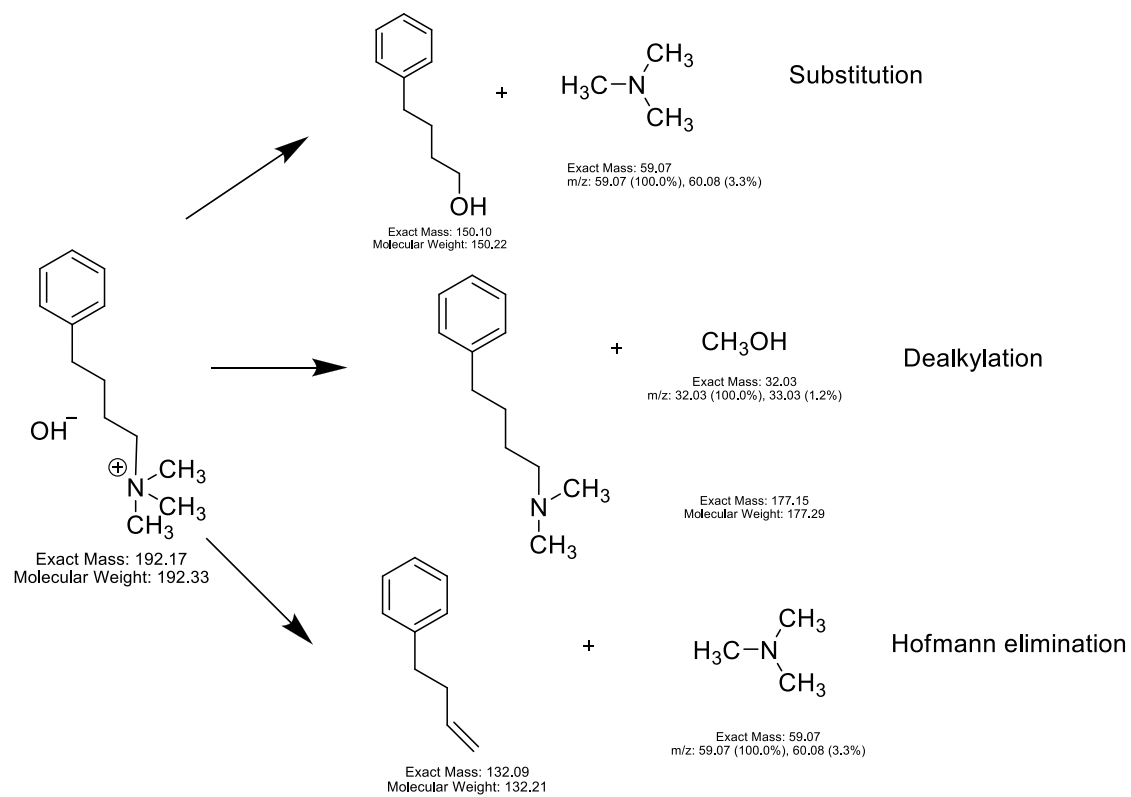


Figure A-8. Degradation mechanisms for sample 4QA1.

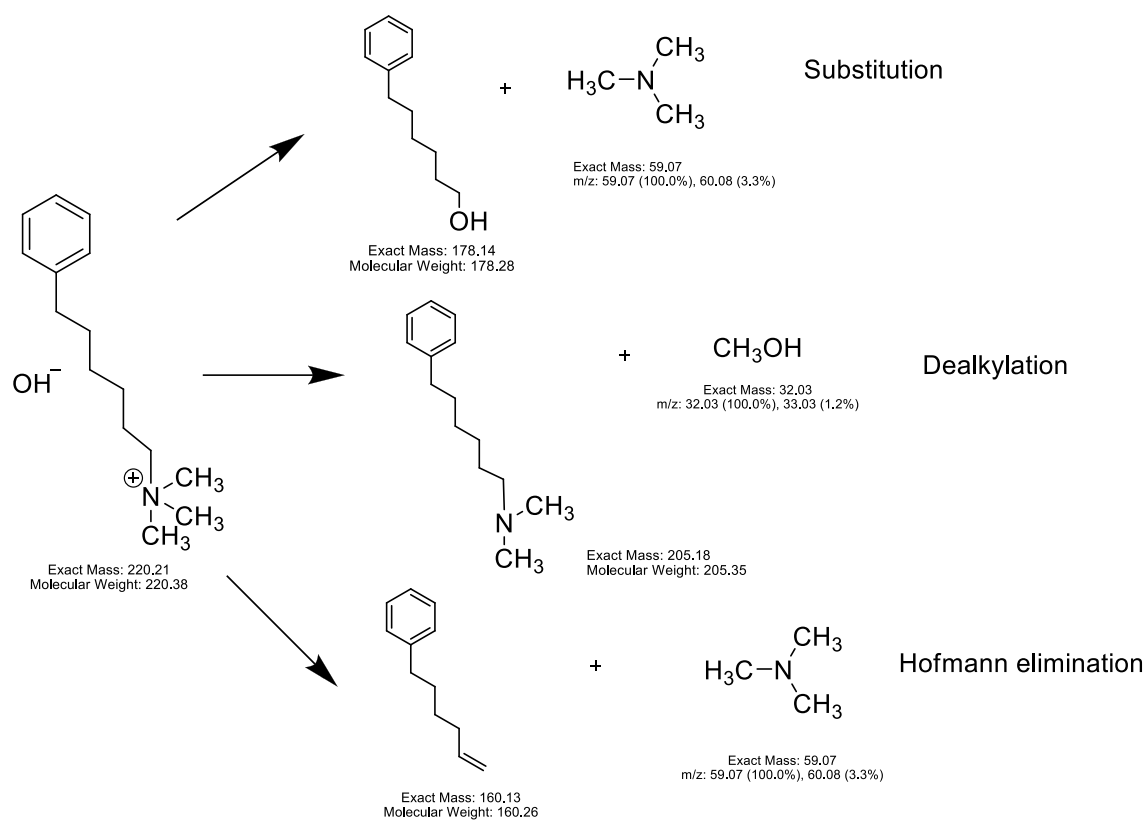


Figure A-9. Degradation mechanisms for sample 6QA1.

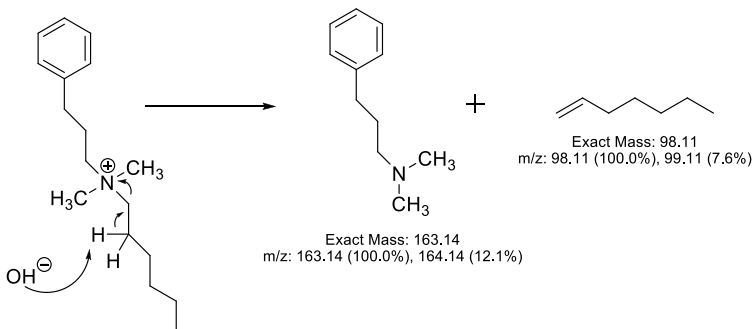
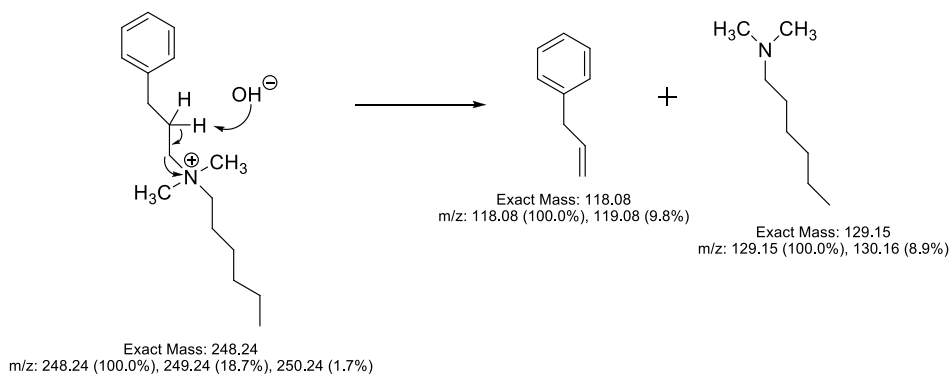
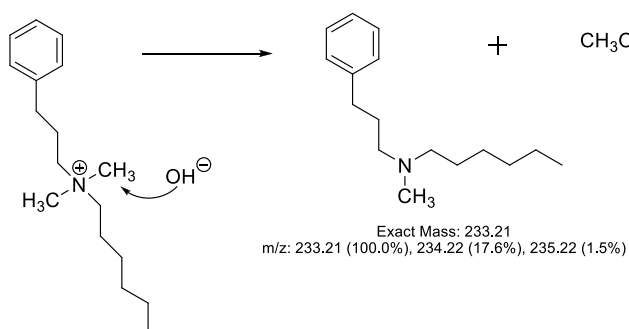
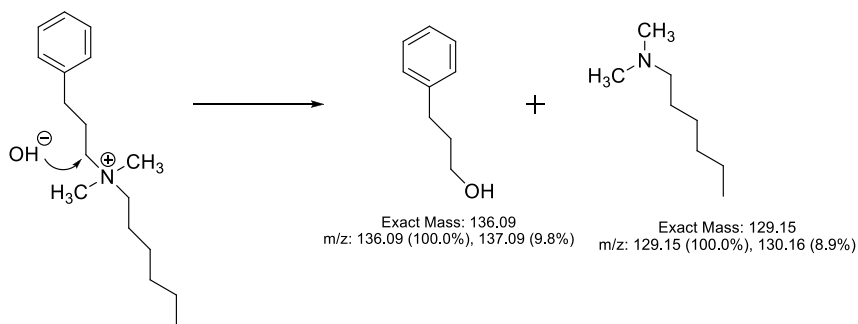


Figure A-10. Degradation mechanisms for sample 3QA6.

Degradation profile of samples 3QA1, 4QA1 and 3QA6:

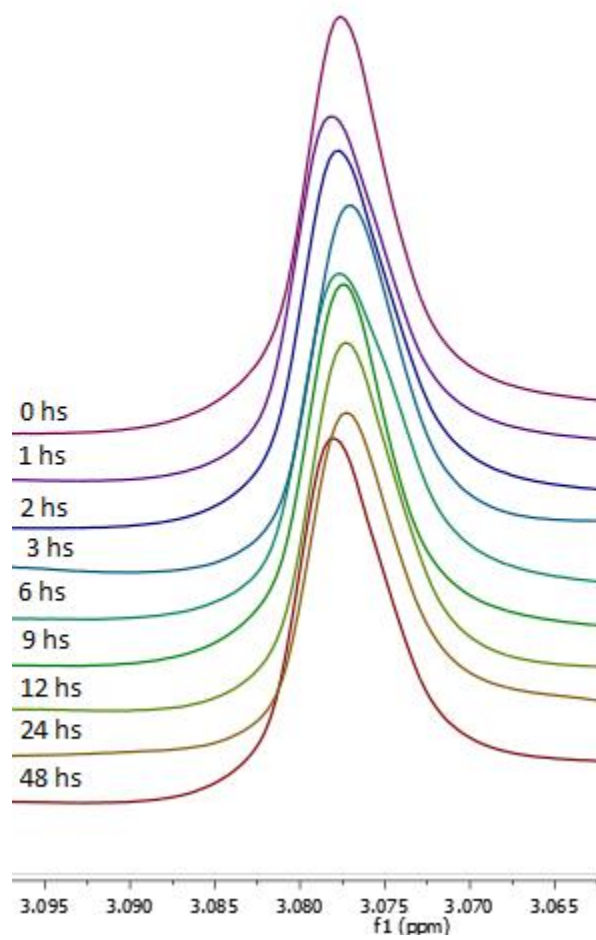


Figure A-11. Degradation profile of the TMA moiety for sample 3QA1.

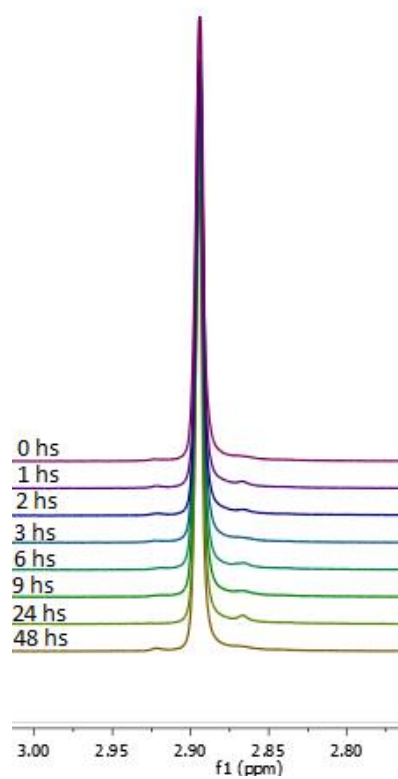


Figure A-12. Degradation profile of the TMA moiety for sample 4QA1.

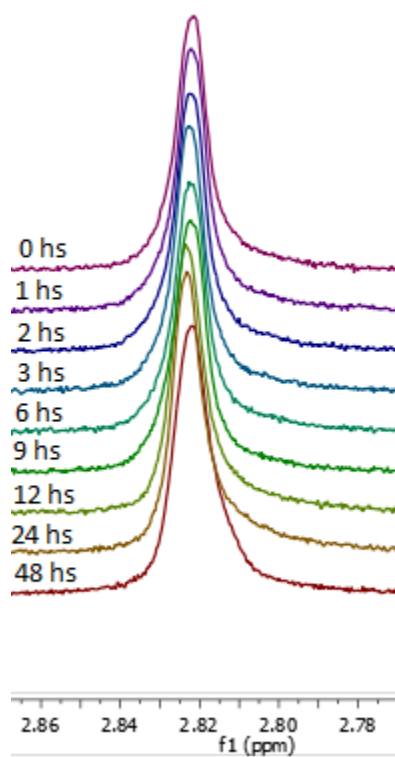


Figure A-13. Degradation profile of the TMA moiety for sample 3QA6.